HINDERED ROTATION OF DIATOMIC MOLECULES IN INERT GAS MATRICES

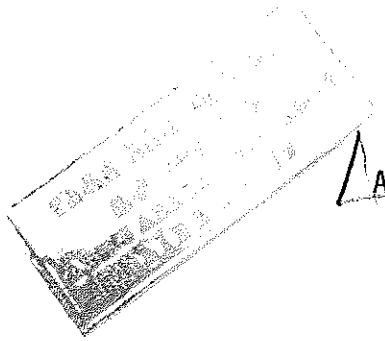

BY

AYELE ABEBE

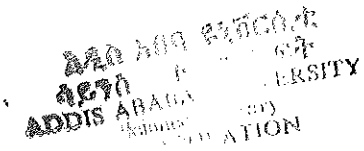

A Thesis

presented to the

School of Graduate Studies

and

The Faculty of Science

Addis Ababa University

In partial fulfillment of the

Requirements for the degree

Master of Science in Physics

June, 1992

DEDICATED TO MY COUSIN

YESHIEMEBET BELETE

ACKNOWLEDGEMENTS

I wish to express my sincere thanks to my Instructor and Advisor, Dr. A.M. Tolkachev, without his excellent guidance, cooperation and frequent advice this work would not have been accomplished.

I am also grateful to my Instructors in the Department of Physics, AAU, for their unreserved help and guidance they gave me during my study.

I would like to record my indeptedness to my family members for their unlimited support and encouragement whenever I needed it. My acknowledgement also goes to all others who contributed in some way to the completion of this work.

Last but not least I would like to extend my thanks to Ato Girma Dagne of the Physics Department who painstakingly done the technical part of the thesis.

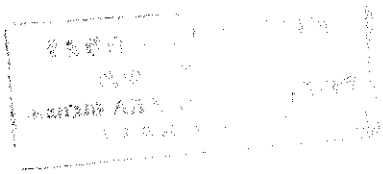

ABSTRACT

The hindered rotation of the diatomic molecuel Co in solid Ar matrix is discussed by propesing the distortion of the octahedral symmetry of the crystal field of the matrix in the vicinity of the impurity molecule to a lower symmetry, in particular tetrahedral symmetry. The solutions of the Schrödinger equation are obtained in general form using group theory analogous to the well known Devonshire model.

Numerical calculations of the energy levels and heat capacity for Co molecules in Ar are made for different strength of the crystal field. Qualitative agreement with experimental data in the temperature range 0.5 - 10K is achieved. Parameters characterizing the hindered rotation of Co molecule in Ar are predicted.

CONTENT

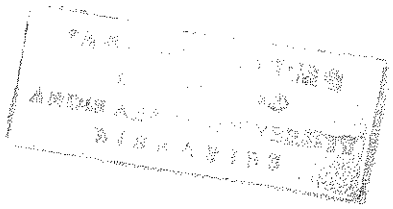

INTRODUCTION

The main aim of this theoretical work is to investigate the hindered rotation of diatomic molecules in crystal fields by determining the rotational energy states of the molecules that are trapped in the Inert gas matrices (cryocrystals). This help us to get an accurate information about the rotational barriers and intermolecular forces. This in turn has got application in understanding the thermal and thermodynamic properties of the solid solutions (impurity molecules in inert gas matrices) such as heat capacity, linear expansion, dielectric constant and others; due to the fact that at low temperature rotational excitations are dominant and greatly influence these properties.

Various experimental methods are employed to study the rotational motion of molecules in solids using infrared absorption, thermal conductivity and specific heat measurements at low temperatures on crystal doped with impurity molecules.

Many attempts are being done to interpret experimentally observed results using theoretical models. The first mathematical treatment of the problem was done by L. Pauling (1930)[1]. All such attempts are primarly concerned in solving the Schrodinger equation for a diatomic molecule placed inside a crystal for a known symmetry of crystal potential field. Usually the nature and magnitude of this crystal field can not be accurately known due to the various interactions of the impurity molecules and the host crystal atoms; as a consequence of which the solutions of the Schrodinger equation may not adequately describe all observed experimental investigations.

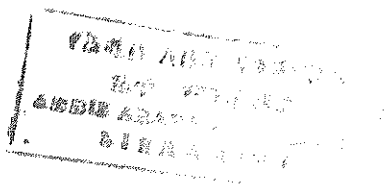

Since it is quite complicated to solve directly the Schrodinger equation for our system under study, we used throughout our work a group theoretical analysis inorder to simplify the steps towards the solution of the Schrodinger equation. The role of symmetry and group theory in facilitating the steps to obtain the eigenfunctions and eigenvalues of the Schrodinger equation is presented in the first chapter.

In Chapter II we dealt about the rotation of diatomic molecules in a field of octahedral symmetry, known as the Devonshire model. Comparison of experimental results obtained from heat capacity and thermal expansion measurements on inert gas crystals such as Ar and Kr with impurity diatomic molecules of $^{14}N_2$, $^{15}N_2$ and CO at low temperatures (2k to 12k) with the calculated values of the Devonshire model reveals the shortcomings of the model.

In Chapter III, an extended model, the Devonshire-Manz-Mirsky (DMM) model will be treated. Though the DMM model takes into account factors which are ignored by Devonshire model such as host lattice relaxations or pseudorotation of cage, but still retains the octahedral symmetry of the field, is unable to give even a qualitative description for the results of thermal exapnsion measurements at low temepratures. Despite this, it worthmentioning that both qualitative and quantitative descriptions of experimental results on measurements of heat capacity at low temperatures (2k to 12k) on different solid solutions of inert gases could be very well understood in terms of this modified model.

The inadequacy of DMM model in interpreting some experimental results may be, among many other reasons, due to its consideration of the symmetry

the crystal field to remain unchanged even when lattice distortion is evident. As pointed out by Manz and Mirsky[14] themselves, the lattice atoms always relax into new momentary equilibrium for a given momentary molecular orientation. But these equivalent reorientations of the atoms may not lead to restore their original symmetry from pure geometrical considerations. Such distortions suggest the original symmetry of the local field to be replaced by other lower symmetry and motivated us to propose the distorted configuration to posses another symmetry, for example a tetrahedral symmetry rather than octahedral symmetry.

The rotation of diatomic molecules in a potential field having tetrahedral symmetry is discussed in Chapter IV. We tried to justify our proposal of the tetrahedral symmetry by the help group theory. Corresponding rotational wave functions and energy eigenvalues are computed. The results of our heat capacity calculations are compared with recent experimental values for heat capacity measurements available from literatures. Finally, conclusions and remarks are made in Chapter V.

CHAPTER I

ROLE OF SYMMETRY AND GROUP THEORY

1.1 Point Group Representations

A transformation of a system to a position that is physically undistingushable from its original position is accomplished through appropriate symmetry operations. Such operations could be performed with respect to a point, a line or a plane. The set of all symmetry transformations which leaves a given system invariant constitute the group of symmetry of that system. In all subsequent discussions, the group of symmetry referred indicate the molecular point group of the system under consideration, i.e., all possible rotations, reflections and inversion which keep the system invariant when applied about the molecular crystal axes.

Elements of a point group could be expressed either by the symmetry operations or by the square matrices corresponding to the symmetry operators. It is evident that these matrices also form a group which is isomorphic to the group of the symmetry operations which could be checked by listing the product of all pairs of elements, or by constructing the multiplication tables.

Consider as example a point group whose symmetry elements are C_n axes and $3\sigma v$ plane, a $\tilde{C}_{3v}$ point group. The symmetry operators are given by $\hat{E}$, $\hat{C}_3$, $\hat{C}_3^2$, $\hat{\sigma}_a$, $\hat{\sigma}_b$, σ_c

$$\hat{E}:\begin{pmatrix}1&0&0\\0&1&0\\0&0&1\end{pmatrix} = I \qquad \hat{C}_3:\begin{pmatrix}-\frac{1}{2}&\frac{1}{2}\sqrt{3}&0\\\frac{1}{2}\sqrt{3}&-\frac{1}{2}&0\\0&0&1\end{pmatrix} = A \qquad \hat{C}_3^2:\begin{pmatrix}-\frac{1}{2}&\frac{1}{2}\sqrt{3}&0\\-\frac{1}{2}\sqrt{3}&-\frac{1}{2}&0\\0&0&1\end{pmatrix} = B$$

$$\hat{\sigma}_a:\begin{pmatrix} \frac{1}{2} & +\frac{1}{2}\sqrt{3} & 0 \\ +\frac{1}{2}\sqrt{3} & -\frac{1}{2} & 0 \\ 0 & 0 & 1 \end{pmatrix} = C \qquad \hat{\sigma}_b:\begin{pmatrix} +\frac{1}{2} & -\frac{1}{2}\sqrt{3} & 0 \\ -\frac{1}{2}\sqrt{3} & -\frac{1}{2} & 0 \\ 0 & 0 & 1 \end{pmatrix} = D \qquad \hat{\sigma}_c:\begin{pmatrix} -1 & 0 & 0 \\ 0 & 1 & 0 \\ 0 & 0 & 1 \end{pmatrix} = F \qquad (1.1)$$

Any set of non-null square matrices which have the same multiplication table structure or form as that of the table of the symmetry operations of a given group is known as the representation of the group. The order of these matrices gives us the dimension of the representation.

It is quite interesting to note that in addition to the matrices in Eq.(1), we can also construct other set of new matrices which multiply in the same manner as the operators of the group by subjecting each matrix I, A, B, C, D, F to a passive trasformation of the type

$$U^{-1}IU,\ U^{-1}AU,\ U^{-1}BU,\ C^{-1}CU,\ U^{-1}DU,\ U^{-1}FU \qquad (1.2)$$

where U is any non-singular matrix of the same order. This way we can obtain an infinite number of representations to a given point group.

Additional representations of the point-group can be obtained by noting the block diagonal form of the matrices in Eq.(1). Partitioning these matrices into submatrices as given below, we get a set of matrices which multiply in the same way as those in Eq.(1) or (2).

$$I'=\begin{pmatrix} 1 & 0 \\ 0 & 1 \end{pmatrix} \qquad A'=\begin{pmatrix} -\frac{1}{2} & -\frac{1}{2}\sqrt{3} \\ \frac{1}{2}\sqrt{3} & -\frac{1}{2} \end{pmatrix} \qquad B'=\begin{pmatrix} -\frac{1}{2} & \frac{1}{2}\sqrt{3} \\ -\frac{1}{2}\sqrt{3} & -\frac{1}{2} \end{pmatrix}$$

$$C'=\begin{pmatrix} \frac{1}{2} & \frac{1}{2}\sqrt{3} \\ \frac{1}{2}\sqrt{3} & -\frac{1}{2} \end{pmatrix} \qquad D'=\begin{pmatrix} \frac{1}{2} & -\frac{1}{2}\sqrt{3} \\ -\frac{1}{2}\sqrt{3} & -\frac{1}{2} \end{pmatrix} \qquad F'=\begin{pmatrix} -1 & 0 \\ 0 & 1 \end{pmatrix} \qquad (1.3)$$

c) The condition that must be satisfied by two distinct irreducible representations i and j is that

$$\sum_{\hat{R}} x_i^*(\hat{R})\, x_j(\hat{R}) = h\,\delta_{ij} \tag{1.5}$$

where $x_i(\hat{R})$ and $x_j(R)$ are the characters of the operator $\hat{R}$ in the i and j representations respectively and h is the total number of the symmetry operators in the group. Note that for an irreducible representation we always have

$$\Sigma |x_i(\hat{R})|^2 = h \tag{1.6}$$

The molecular point groups which are found to be the most important in the study of the rotation of diatomic molecules in cystals include the octahedral group (O_h) the tetrahedral group (T_d) and the two lower symmetries which result from slight distortion of the octahedral group, i.e., tetragonal and trigonal groups.

The octahedral group O_h is the largest of all point groups comprising 48 elements (24 proper and 24 improper rotations). These include the identity operator E, eight proper rotations by 120° about the cube diagonals ($8C_3$), 6 proper rotations by 180° about axes through the origin parallel to the face diagonals ($6C_2$), six proper rotations by 90° about the coordinate axes ($6C_4$) and three proper rotations by 180° about the coordinate axes ($3C_2$) which form the O group. The remaining 24 elements are O x i where i is the inversion operator, i.e., iE, $8iC_3$'s, $6iC_2$'s, $6iC_4$'s and $3iC_2$'s.

If six atoms are placed equidistant on either sides of the coordinate

axes from a common origin the resulting space figure will be that of a regular octahedron and the group of all symmetry operation of it constitute the O_h group, see Fig.1. As shown in the figure, an octahedron has the same symmetry elements as a cube.

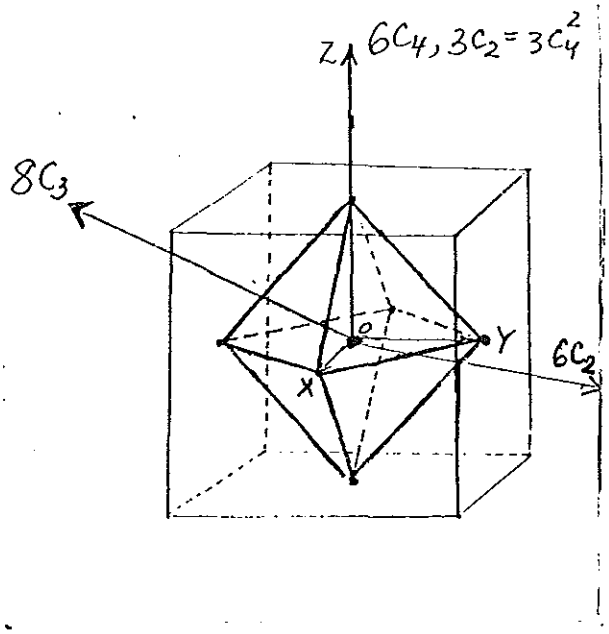

Fig.1a

Fig.1a: Rotational Symmetries of an octahedron

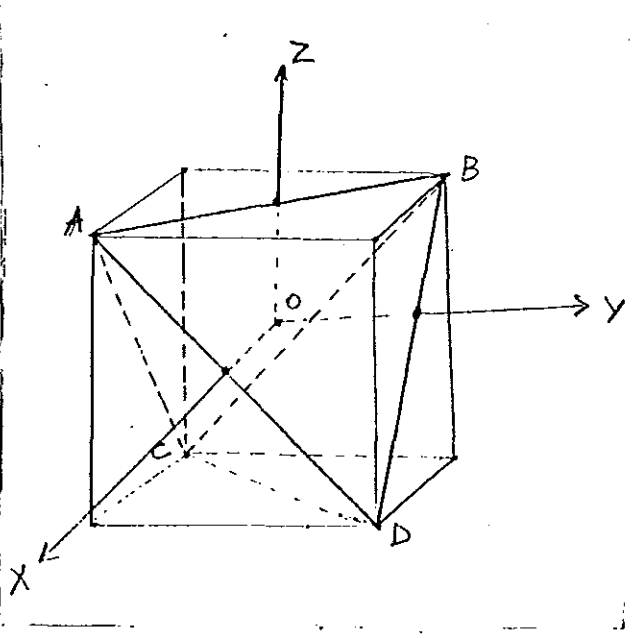

Fig.1b

Fig.1b: Tetrahedron inscribed in cube

Figure 2 shows a regular tetrahedron ABCD inscribed in a cube. The set of operations which take the tetrahedron into itself constitute the tetrahedral point group T_d. This point group consists of 12 proper rotational operations of the T group and 12 improper rotations i x T. The proper rotations include E, $3C_2$'s about the x,y,z axes respectively, $8C_3$'s about the body diagonals of the cube.

The representations and group characteristics for both octahedral and tetrahedral point group are given in tables I and II. Using the notations used by Mulliken the types of conventions used for the irreducible repre-

sentations are

a) A,E and T stands for one, two and three dimensional irreducible representations respectively.

b) If the irreducible representation is invariant under inversion we add the subscript g and if not u.

c) If two non-equivalent irreducible representaitons are not distringuished by the above rules we add numerical subscripts to differentiate them.

O_h	E	$3C_2$	$6C_4$	$6C_2$	$8C_3$	iE	$3iC_2$	$6iC_4$	$6iC_2$	$8iC_3$
A_{1g}	1	1	1	1	1	1	1	1	1	1
A_{1u}	1	1	1	1	1	−1	−1	−1	−1	−1
A_{2g}	1	1	−1	−1	1	1	1	−1	−1	1
A_{2u}	1	1	−1	−1	1	−1	−1	1	1	−1
E_g	2	2	0	0	−1	2	2	0	0	−1
E_u	2	2	0	0	−1	−2	−2	0	0	1
T_{1g}	3	−1	1	−1	0	3	−1	1	−1	0
T_{1u}	3	−1	1	−1	0	−3	1	−1	1	0
T_{2g}	3	−1	−1	1	0	3	−1	−1	1	0
T_{2u}	3	−1	−1	1	0	−3	1	1	−1	0

Table I. Representations of O_h group[1]

	Characters				
Type	E	$3C_2$	$6iC_4$	$6iC_2$	$8C_3$
A_1	1	1	1	1	1
A_2	1	1	−1	−1	1
E	2	2	0	0	−1
T_1	3	−1	1	−1	0
T_2	3	−1	−1	1	0

Table II. Representations of T_d group

1.2 Advantage of Group Theoretical Analysis

A prior knowledge of how the atoms in a given crystal are configurated facilitates the proper choice of the symmetry operations (operators) which leave the Hamiltonian of the system invariant. Once this is known, the rotation of a molecule substitutionaly placed at one of the lattice points inside the crystal could be investigated by the help of group theory.

The Hamiltonian of our system is specified relative to the equilibrium

nuclear configuration of the crystal atoms which in turn define its point group and the corresponding symmetry operations, say $\hat{R}$, $\hat{S}$, $\hat{T}$, ... or operators $\hat{O}_R$, $\hat{O}_S$, $\hat{O}_T$.... which operate on functions of coordinates.

The time-independent Schrodinger equation is given by

$$\hat{H}\,\psi_{j,\nu} = E_\nu\,\psi_{j,\nu} \tag{1.7}$$

where $j = 1,2, \ldots n$ distinguishes wave functions belonging to the energy level ν. Now since the symmetry operations (operators) we employ leave the Hamiltonian invariant

$$\hat{O}_R(\hat{H}\,\psi_{j,\nu}) = \hat{H}\hat{O}_R\,\psi_{j,\nu} \tag{1.8}$$

it follows then

$$[\hat{O}_R,\hat{H}] = 0 \tag{1.9}$$

using Eq.(8) and the fact that symmetry operators are linear operators

$$\hat{H}(\hat{O}_R\,\psi_{j,\nu}) = E\,(\hat{O}_R\,\psi_{j,\nu}) \tag{1.10}$$

which tells us that $\hat{O}_R\,\psi_{j,\nu}$ is an eigenfunction of $\hat{H}$ with the same eigenvalue E_ν, and hence it should be the linear combination of the n eigenfunctions belonging to E_ν. Therefore,

$$\hat{O}_R\,\psi_{j,\nu} = \Sigma\,\psi_{i,\nu}\,\gamma_{ij,\nu} \tag{1.11}$$

where γ_{ij} are a set of n^2 constants which describe how the operator $\hat{O}_R$ transform each of the n wave functions $\psi_{i,j}$. These constants could be represented by n x n square matrix R. Similarly for other operators of

the point group corresponding square matrixes could be known.

For a given n-fold degenerate energy level, the set of n linearly independent wavefunctions $\psi_{1,\nu}, \psi_{2,\nu} \cdots \psi_{n,\nu}$ are transformed into linear combination of one another by the symmetry operations (Eq.(1.11)), these n wavefunctions constitutes a basis for some particular representation Γ_ν of the point group.

There is a unique representation of the group of the Schrodinger equation corresponding to each eigenvalue of the Hamiltonian. Knowing the dimensions of all the irreducible representations of a group of schrodinger equation, we can tell with no doubt the degrees of degeneracy possible in any problem[2]. It follows then a perturbation can lift degeracies iff its inclusion in the Hamiltonian changes the irreducible representation.

Let us consider a demonstrative example to exhibit the power of group theoretical analysis in determining how each rotational energy levels split i.e., the lifting of the degeneracies associated with the levels under a crystal field of known symmetry. At this stage, it is necessary to note that the magnitude of such splittings could not be calculated unless an explicit expression of the crystal field is known.

1.3 Splitting of Energy Levels Under Crystal Field

When an atom or molecule is placed in a crystal various inhomogeneous electric fields act up on it. These fields will eventually distroy the isotropy of the free space. As a consequence, the symmetry group is reduced

from a full 3-dimensional rotation group and inversion to finite group of rotation and perhaps reflections. The free atom or molecule irreducible representation of the full rotation group which is based on spherical harmonics or angular momentum eigenfunction will be reduced with respect to such subgroup.

This reduction of the dimension of the original irreducible representation causes the degeneracy associated with the full rotational symmetric group to be lifted. In other words, the free atom/molecule energy levels will be splitted by the crystalline field. As pointed out by Bethe[3] the degree of residual degeneracy is determined from the symmetry by the group theory with ultimate accuracy since no perturbation theory approximation is used.

Furthermore, consider the case of intermediate crystal field splitting, i.e., when the crystal field splitting is between the spin-orbit energy and the separation of L-S term in the free atom case. Here the quantum numbers L and S remain good quantum numbers but not J. The crystal field which acts on the orbital motion of the electrons will split the (2L + 1) fold degeneracy. If the symmetry of the crystalline field is known to be an octahedral field, then the symmetry of the problem could be described by O_h group. Recalling $O_h = O \times i$, we can use only the 24 proper rotation of the O group since the addition of inversion to form O_h bring no change. The character of O group is given below in Table III.

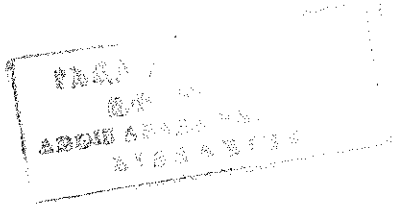

O		E	$8C_3$	$3C_2$	$6C_2$	6C
Γ_1	A_1	1	1	1	1	1
Γ_2	A_2	1	1	1	-1	-1
Γ_3	E	2	-1	2	0	0
Γ_4	T_1	3	0	-1	-1	1
Γ_5	T_2	3	0	-1	1	-1

Table III. Character table of O group

Let us consider an atomic term with angular momentum L. The spherical harmonic $Y_L^M(\theta,\phi)$ which are (2L+1) fold degenerate in isotropic space form a basis for a representation D_L of the rotational group. Now in the presence of the crystalline field, the isotropy of the field will be destroyed and the representation of the full group of all proper rotations will be reduced to a smaller subgroup which are expressible using some of the linear combinations of spherical harmonics. What is necessary to know at this point is the characters of the Γ_i representation and the decomposition formula.

The character of all the classes of a group element in D_L is given by

$$x_L(\phi) = \frac{\sin (L + \frac{1}{2})\phi}{\sin \phi/2} \qquad (1.12)$$

where ϕ is the angle of the proper rotation; which yields for D_L the following values of the characters.

$$
\begin{aligned}
x_L(E) &= 2L + 1 \\
x\ (C_2) = x(\pi) &= (-1)^L \\
x\ (C_3) = x\left(\tfrac{2\pi}{3}\right) &= \begin{cases} 1 & L = 0,3, \ldots \\ 0 & L = 1,4, \ldots \\ -1 & L = 2,5, \ldots \end{cases} \\
x\ (C_4) = x\left(\tfrac{\pi}{2}\right) &= \begin{cases} 1 & L = 0,1,4,5 \ldots \\ -1 & L = 2,3,6,7, \ldots \end{cases}
\end{aligned}
\tag{1.13}
$$

The decomposition formula is given by

$$D_L = \Sigma\ a_i\ r_i \tag{1.14}$$

where

$$a_i = \frac{1}{h}\ \sum_k N_k\ x_i(\ell_k) x\ (\ell_k) \tag{1.15}$$

where h is the total number of the symmetry elements, ℓ_k is the k symmetry operation, N_k is the number of a given rotational symmetry operation and $x_i(\ell_k)$ and $x_L(\ell_k)$ are the character of the ℓ_k operation in the r_i and D_L representation respectively.

Below are the characters tabulated for the first few of these representation of the O group. Then inspect what row of the irreducible representation r_i are added in order to get to which row of D_L representation they correspond. By doing so we can obtain a qualitative information about the splitting of the energy levels.

O	E	$8C_3$	$3C_2$	$6C_2$	$6C_4$
D_0	1	1	1	1	1
D_1	3	0	-1	-1	1
D_2	5	-1	1	1	-1
D_3	7	1	-1	-1	-1
D_4	9	0	1	1	1

Table IV. Characters of O group in D_L representation

How each energy level split under the octahedral field is schemetically given in Table V. Note that only levels with L = 2,3 and 4 are split under the field.

L	
0	$\rightarrow A_1$
1	$\rightarrow T_1$
2	$\rightarrow E + T_2$
3	$\rightarrow A_2 + T_1 + T_2$
4	$\rightarrow A_1 + E + T_1 + T_2$

Table V. Splitting of the rotational energy levels

Moreover, the degenerate levels likely split to other states by considering other lower crystal field symmetries which result due to small fluctuation or departures from the proposed symmetry of lattice sites. These further splittings could be analysed by knowing the correct form of smaller group or the reduced rotational symmetry of the group and by

treating the problem step by step.

For example, from the above result for L = 2 ($D_2 = E + T_2$), a trigonal distortion produce a splitting of the triply degenerate T levels of the octahedral field into a doubly degenerate and a non degenerate level.

$$T_1 \rightarrow E + A_2$$
$$T_2 \rightarrow E + A_1$$

The procedure we used for the determination of the splitting of levels due to crystal fields is schemetically shown below for octahedral and trigonal field.

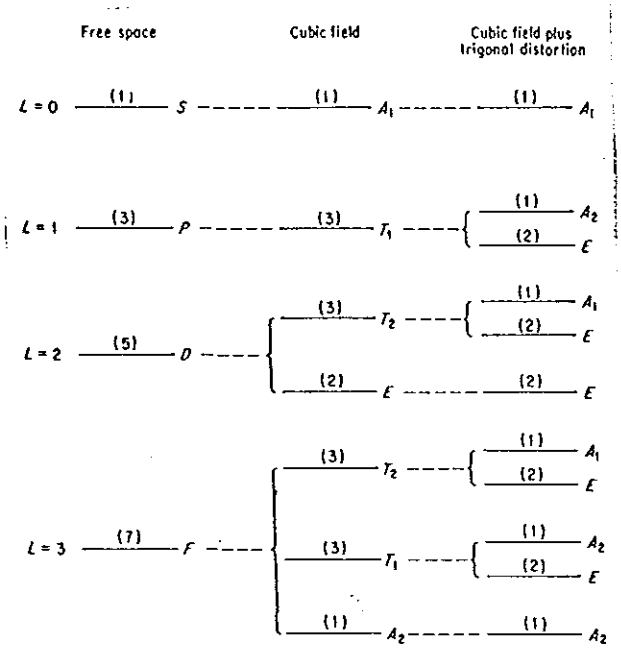

Fig.2. Splitting of levels under octahedral field and trigonal distortion[2]

The discussion of this section clearly shows us two important outcomes which could be employed in the treatment of the rotation of a molecule in

a crystal field in the preceeding chapters; first, the degree of residual degeneracy of a molecular or atomic level in a given field of definite symmetry could be obtained by the use of group theory. Secondly, the various irreducible representation of a point group automatically gives indication how the set of degenerate eigenfunctions transform or what symmetry they have.

CHAPTER II

HINDERED ROTATION OF DIATOMIC MOLECULES IN CRYSTAL FIELD OF OCTAHEDRAL SYMMETRY

A search for the knowledge of the rotational energy states of a rotating molecule in a crystal field is quite essential in understanding the various properties of a solid solution. The obstacle towards the understanding of these energy states lie on one hand, how to solve the corresponding Schrodinger equation directly which is usually complicated. Means of simplification of the problem as the same time obtaining accurate results is cumbersome. On the other hand the exact nature and magnitude of the field could not be easily found. To this end, many procedures, models and approximations are employed in order to justify the experimental results obtained.

In attempt to give a clear picture of the rotation of impurity molecule under the influence of crystal potential considerable research have been done by many scientists since the first time the problem was suggested by L. Pauling. Earlier treatments took the crystal potential to depend only on one angular coordinate.

A more general approach which took both angular coordinates into consideration in a crystal field of definite symmetry gives us a better understanding of the problem. Among such approaches is the one proposed by A.F. Devonshire (1936)[1]. He investigated the rotation of impurity diatomic molecules in a crystal field of octahedral symmetry which is a suitable representation of the field under which molecules move in a cubic crystals.

2.1 Devonshire Model

In this model, Devonshire assumed the molecular impurity to be fixed to a lattice site of the host crystal, and its free rotational motion to be hindered by potential due to lattice forces. He neglects lattice vibrations and possible lattice distortion due to the impurity, potential to be stationary and show the symmetry of the lattice.

Consider a diatomic molecule whose moment of inertia is I, rotating under the influence of a potential energy $V = V(\theta,\phi)$ having an octahedral symmetry. The time independent Schrodinger equation is given by

$$\hat{H}\psi = E\psi \tag{2.1}$$

or in spherical polar coordinate this becomes

$$\frac{-\hbar^2}{2\mu}\left[\frac{\partial^2}{\partial r^2} + \frac{2}{r}\frac{\partial}{\partial r} + \frac{1}{r^2}\frac{\partial^2}{\partial\theta^2} + \frac{1}{r^2\sin\theta}\frac{\partial}{\partial\theta} + \frac{1}{r^2\sin^2\theta}\frac{\partial^2}{\partial\phi^2}\right]\psi + V\psi = E\psi \tag{2.2}$$

since the internuclear distance r is fixed, the rotation of diatomic molecules is taken as rotation with two degrees of freedom; θ and ϕ describing the orientation of the molecular axes relative to the crystallographic axes. Hence, Eq.(2.2) reduces to

$$\left[\frac{1}{\sin\theta}\frac{\partial}{\partial\theta}\left(\sin\theta\frac{\partial\psi}{\partial\theta}\right) + \frac{1}{\sin^2\theta}\frac{\partial^2\psi}{\partial\phi^2}\right] + \frac{8\pi^2 I}{\hbar^2}(E - V(\theta,\phi))\psi = 0 \tag{2.3}$$

where the bracketed term gives us the rotational kinetic energy operator of the molecule. The potential energy $V = V(\theta,\phi)$ which reflects the symmetry of the system could be expanded in a series of surface harmonics

or set of angular momentum eigenfunctions since they span irreducible representations of the full inversion-rotation group that include O_h as a subgroup. In addition $V(\theta,\phi)$ is invariant under the symmetry operations of the O_h group and transform according to the totally symmetric representation A_{1g}.

$$V(\theta,\phi) = \Sigma\ a_{\ell m} Y^{D}_{\ell m} \tag{2.4}$$

where $Y_{\ell m}$ are spherical harmonics of the D representation.

Bethe[3] has proved that there are no spherical harmonics of degree less than four which have octahedral symmetry. An obvious choice and the simplest one for the form of the potential will then be the first non-constant term of the series having the required symmetry which is:

$$V(\theta,\phi) = -\frac{2}{3}\sqrt{\pi}\, k[Y^{4}_{o} + \frac{5}{14}(Y^{4}_{4} + Y^{-4}_{4})]$$

or

$$V(\theta,\phi) = -\, k[P^{o}_{4}(\cos\theta) + \frac{1}{168} P^{4}_{4}(\cos\theta)\, \cos 4\theta] \tag{2.5}$$

where k is a constant which indicate the depth or strength of such potential barrier and $P^{m}_{\ell}(\cos\theta)$ are the associated legendre polynomials. More explicitly Eq.(2.5) could be written as

$$V(\theta,\phi) = -\, k[\frac{1}{8}\ \{3-30\cos^{2}\theta + 35\cos^{4}\theta + 5\sin^{4}\theta\ \cos^{4}\phi\ \}] \tag{2.6}$$

The nature of the potential in which the impurity diatomic molecule moves could be studied using Eqs. (2.5) or (2.6). The projection of the equipotential lines on the plane $\theta = \pi/2$ is given in Figure 4.

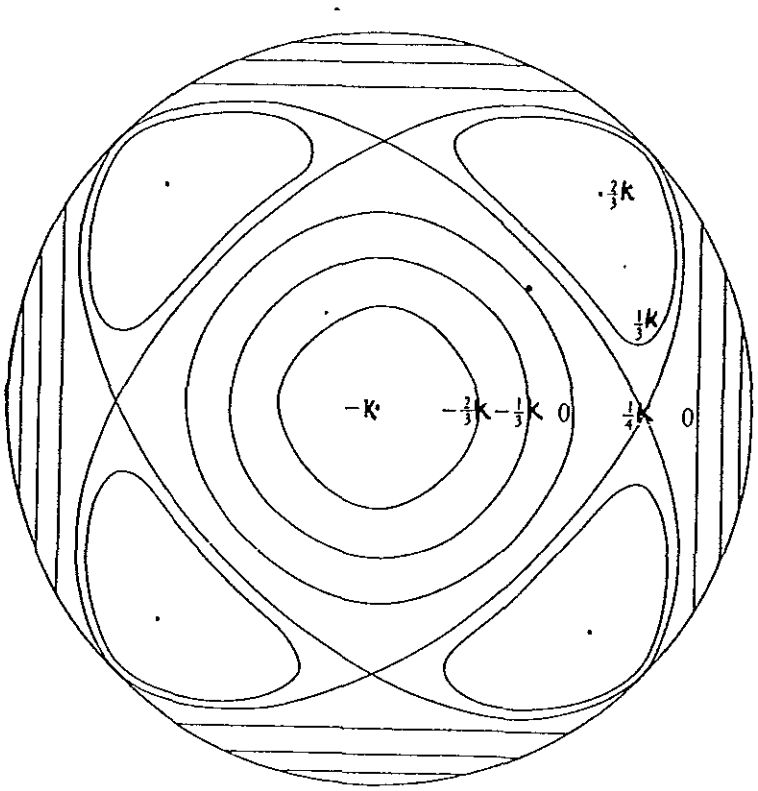

Fig.3. Equipotential lines [from reference 1]

For positive values of the potential barrier parameter k, the potential has six minima equal to -k at

$$\theta = 0 \quad \text{or} \quad \pi \ , \ \pi/2 \qquad \phi = 0, \pm \frac{\pi}{2} \quad \text{or} \quad \pi$$

Since the impurity diatomic molecule is substitutionally placed at one of the lattice sites of the host crystal which form an octahedron for a unit cell, the six minimum points correspond to the configuration when the molecule is located at one of the six faces of the cube in which the octahedron is inscribed as shown in Fig.4a.

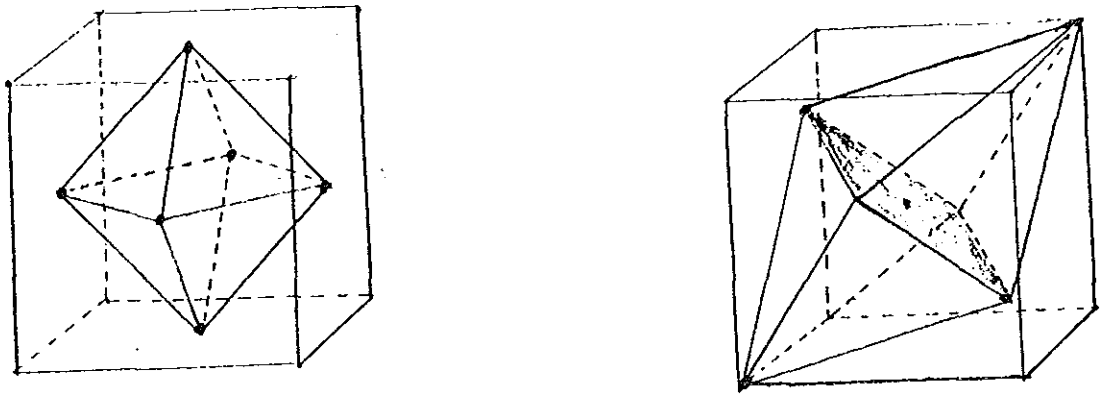

(a) (b)

Fig.4. The impurity molecule located at one of the six faces of the cube (a) and at one of the corners of a cube (b).

The potential energy $V(\theta,\phi)$ has eight maxima equal to 2/3k at

$$\theta = \cos^{-1} \pm \frac{1}{\sqrt{3}} \qquad \phi = \pm \frac{\Pi}{4} \text{ or } \pm \frac{3\Pi}{4}$$

and these correspond to the configuration when the molecule is found at any one of the eight corners of the cube as shown in Fig.5b.

The dividing line between the potential maxima and minima is the equipotential curve $V = \frac{1}{4}k$. Hnece, the depth of the six potential hollows will be $\frac{5}{4}k$ and the eight potential hills will have a depth of $\frac{5}{12}k$.

Coming back to the main task of solving the Schrodinger equation

$$\frac{1}{\sin\theta}\frac{\partial}{\partial\theta}\left(\sin\theta\frac{\partial\psi}{\partial\theta}\right) + \frac{1}{\sin^2\theta}\frac{\partial^2\psi}{\partial\phi^2} + \frac{8\Pi^2 I}{h^2}(E-V(\theta,\phi))\psi = 0 \qquad (2.7)$$

this equation is invariant under the operations of the O_h group, i.e.,

$$[\hat{H}, \hat{O}_R] = 0 \qquad \{\hat{O}_R\} = O_h \tag{2.8}$$

so that the eigenfunctions of the Hamiltonian could be chosen to be that of the symmetry operations of the group. In other words, any energy eigenfunction could be expressed as a linear combination of spherical harmonics $P_\ell^m(\cos\theta)\cos m\phi$. It should be known that the surface harmonics can not be simply assigned to any representation of O_h, we must obtain the correct linear combination of them for a given representation so that the eigenfunction will be the solution of the Schrodinger equation.

$$\psi^D = \sum_{\ell,m} a_{\ell m} Y^D_{\ell m} \tag{2.9}$$

where ψ^D is the eigenfunction for a given D representation, $a_{\ell m}$ are constants, $Y^D_{\ell m}$ is the spherical harmonics of a representation D and ℓ, m are running index.

The solutions of the Schrodinger equation which are the eigenfunctions of the Hamiltonian corresponding to a definite energy level will form a representation of the octahedral symmetry. As shown in section 1.1 Tab.I O_h group has ten distinct irreducible representations and hence ten different symmetry species of energy eigenfunctions are possible. Therefore, each energy level could be specified with respect to the symmetry type of irreducible representation the eigenfunctions span.

In search of the proper series of the spherical harmonics which satisfy the Schrodinger equation, Devonshire employed the series of spherical harmonics of the tetragonal point group D_{4h} which were known prior to

his work given in Table VI.

O_h		D_{4h}	O_h		D_{4h}
A_{1g}	→	A_{1g}	A_{1u}	→	A_{1u}
A_{2g}	→	B_{1g}	A_{2u}	→	B_{1u}
E_g	→	$A_{1g} + B_{1g}$	E_u	→	$A_{1u} + B_{1u}$
T_{1g}	→	$A_{2g} + E_g$	T_{1u}	→	$A_{2u} + E_u$
T_{2g}	→	$B_{2g} + E_g$	T_{2u}	→	$B_{2u} + E_u$

Tab.VI. Correspondence between representations of O_h and D_{4h}.

Such a correspondence is possible since O_h has a complete symmetry of the D_{4h}[4]. So if a series for a given representation of D_{4h} is known, then it will be also the correct series to one of the O_h representation to which it correspond or it will be one of the pair of solutions of the O_h group. The series of the O_h representation to which the different types of solution of the Schrodinger equation belong are given in Table VII.

D_{4h}	O_h	Series
A_{1g}	A_{1g} or E_g	$a_o^o + a_2^o p_2^o + a_4^o p_4^o + a_4^4 p_4^4 \cos 4\phi + \ldots$
B_{1g}	A_{2g} or E_g	$a_2^2 p_2^2 \cos 2\phi + a_4^2 p_4^2 \cos 2\phi + \ldots + a_6^6 p_6^6 \cos 6\phi$
A_{2g}	T_{1g}	$b_4^4 p_4^4 \sin 4\phi + b_6^4 p_6^4 \sin 4\phi + \ldots$
E_g	T_{1g} or T_{2g}	$a_2^1 p_2^1 \cos\phi + a_4^1 p_4^1 \cos\phi + a_4^3 p_4^3 \cos 3\phi + \ldots$
B_{2g}	T_{2g}	$b_2^2 p_2^2 \sin 2\phi + b_4^2 p_4^2 \sin 2\phi + \ldots$
A_{1u}	A_{1u} or E_u	$b_5^4 p_5^4 \sin 4\phi + b_7^4 p_7^4 \sin 4\phi + \ldots$
B_{1u}	A_{2u} or E_u	$b_3^2 p_3^2 \sin 2\phi + b_5^2 p_5^2 \sin 2\phi + \ldots$
A_{2u}	T_{1u}	$a_1^o p_1^o + a_3^o p_3^o + a_5^o p_5^o + a_5^4 p_5^4 \cos 4\phi + \ldots$
E_u	T_{1u} or T_{2u}	$b_1^1 p_1^1 \sin\phi + b_3^1 p_3^1 \sin\phi + \ldots$
B_{2u}	T_{2u}	$a_3^2 p_3^2 \cos 2\phi + a_5^2 p_5^2 \cos 2\phi + \ldots$

Tab.VII Representations of O_h in spherical harmonics[1]

Note that the coefficients a_ℓ^m , b_ℓ^m in the above series expansion are always chosen in such a way that the series will be the solution of the Schrodinger equation.

Employing the same procedure as used in section 1.3 for determination of how the energy levels split under a crystal field of known symmetry, the rotational energy levels under the octahedral symmetry are split as shown below in Tab.VIII.

ℓ		ℓ	
0	$\rightarrow A_{1g}$	5	$\rightarrow E_u + 2T_{1u} + T_{2u}$
1	$\rightarrow T_{1u}$	6	$\rightarrow A_{1g} + A_{2g} + T_{1g} + 2T_{2g}$
2	$\rightarrow E_g + T_{2g}$	7	$\rightarrow A_{2u} + E_u + 2T_{1u} + 2T_{2u}$
3	$\rightarrow A_{2u} + T_{1u} + T_{2u}$	8	$\rightarrow A_{1g} + 2E_g + 2T_{1g} + 2T_{2g}$
4	$\rightarrow A_{1g} + E_g + T_{1g} + T_{2g}$	9	$\rightarrow A_{1u} + A_{2u} + E_u + 3T_{1u} + 2T_{2u}$

Table VIII. Splitting of levels under octahedral field

Till this stage, we discussed the forms of the eigenfunctions which are solutions of the Schrodinger equation and the scheme of splitting of the rotational energy by the use of group theory by assuming only that the potential has an octahedral symmetry.

The rotational energy values could now be computed by using the potential energy $V(\theta,\phi)$ given in Eq.(2.5) and the series of spherical harmonics for the representation we wish to solve. The Schrodinger equation needed to be solved is

$$\frac{1}{\sin\theta}\frac{\partial}{\partial\theta}\left(\sin\theta\frac{\partial\psi}{\partial\theta}\right)+\frac{1}{\sin^2\theta}\frac{\partial^2\psi}{\partial\phi^2}+\left[w+k\left(p_4^0(\cos\theta)+\frac{1}{168}p_4^4(\cos\theta)\cos 4\phi\right]\psi=0 \qquad (2.10)$$

Where

$$W = \frac{8\pi^2 I E}{h^2} = \frac{E}{B} \qquad k = \frac{8\pi^2 I K}{h^2} = \frac{K}{B} \tag{2.10}$$

and the rotational constant B is defined as $B = \frac{h^2}{8\pi^2 I}$

Upon substitution of the eigenfunctions in Eq.(2.10), we encounter products of spherical harmonics of the type

$$[P_4^0(\cos\theta) + P_4^4(\cos\theta)\cos 4\phi]P_\ell^m \begin{Bmatrix} \cos m\phi \\ \sin m\phi \end{Bmatrix}$$

and are simplified by the following recurrence relations

$$P_4^0 P_\ell^m = \frac{(\ell+m)(\ell+m-1)(\ell+m-2)(\ell+m-3)}{(2\ell-5)(2\ell-3)(2\ell-1)(2\ell+1)} \cdot \frac{35}{8} P_{\ell-4}^m$$

$$+ \frac{(\ell+m)(\ell m-1)(\ell^2-\ell-2-7m^2)}{(2\ell-5)(2\ell-1)(2\ell+1)(2\ell+3)} \cdot \frac{5}{2} P_{\ell-2}^m$$

$$+ \frac{(3\ell^2+6\ell^3-3\ell^2-6\ell-5m^2)(6\ell^2+6\ell-5)+35m^4}{(2\ell-3)(2\ell-1)(2\ell+3)(2\ell+5)} \cdot \frac{3}{4} P_\ell^m$$

$$+ \frac{(\ell+1-m)(\ell+2-m)(\ell^2+3\ell-7m^2)}{(2\ell-1)(2\ell+1)(2\ell+3)(2\ell+7)} \cdot \frac{5}{2} P_{\ell+2}^m$$

$$+ \frac{(\ell+1-m)(\ell+2-m)(\ell+3-m)(\ell+4-m)}{(2\ell+1)(2\ell+3)(2\ell+5)(2\ell+7)} \cdot \frac{35}{8} P_{\ell+4}^m \tag{2.12}$$

$$P_4^4 P_\ell^m = \frac{105}{(2\ell-5)(2\ell-3)(2\ell-1)(2\ell+1)} P_{\ell+4}^{m+4} - \frac{420}{(2\ell-5)(2\ell-1)(2\ell+1)(2\ell+3)} P_{\ell\ 2}^{m+4}$$

$$+ \frac{630}{(2\ell-3)(2\ell-1)(2\ell+3)(2\ell+5)} P_\ell^{m+4} - \frac{420}{(2\ell-1)(2\ell+1)(2\ell+3)(2\ell+7)} P_{\ell+2}^{m+4}$$

$$+ \frac{105}{(2\ell+1)(2\ell+3)(2\ell+5)(2\ell+7)} P_{\ell+4}^{m+4} \qquad (2.13)$$

We are now in a position to obtain the energy values for a given representation. Suppose we wish to find the energy values of A_{1g} representation of the O_h group. The series of A_{1g} is substituted in the Schrodinger equation and use the property of spherical harmonics

$$\left[\frac{1}{\sin\theta}\frac{\partial}{\partial\theta}\sin\theta\frac{\partial}{\partial\theta} + \frac{1}{\sin^2\theta}\frac{\partial^2}{\partial\phi^2}\right] Y_\ell^m(\theta,\phi) = -\ell(\ell+1)\, Y_\ell^m(\theta,\phi) \qquad (2.14)$$

Furthermore, we express all the terms in the equation as the sum of surface harmonics by using Eq.(2.12) and (2.13). By equating the coefficients of each spherical harmonics to zero, a system of linear equations between the coefficents such as given below is obtained.

$$a_o^o W + \frac{1}{9} a_4^o k + \frac{40}{3} a_4^4 k = 0$$

$$a_2 [W - 6 + \tfrac{6}{7} k] + \frac{100}{693} a_4^o k - \frac{800}{33} a_4^4 k + \frac{25}{143} a_6^o k + \frac{9000}{143} a_6^4 k = 0 \qquad (2.15)$$

$$\vdots$$

. etc

The condition for these set of linear equation to be consistent is that the determinant should vanish, thereby the energy values, rather the roots of W is determined as a determinantal equation.

Such calculation is lengthy and quite labourious when computed directly, but by the help of computers the determinant of large dimensions could be solved numerically. In such a way, few of the lowest roots of W corresponding to a representation can be obtained for different values of the constant k by taking the first few rows and columns.

Devonshire's results of the rotational energy values as a function of k = k/B is plotted in Fig.5.

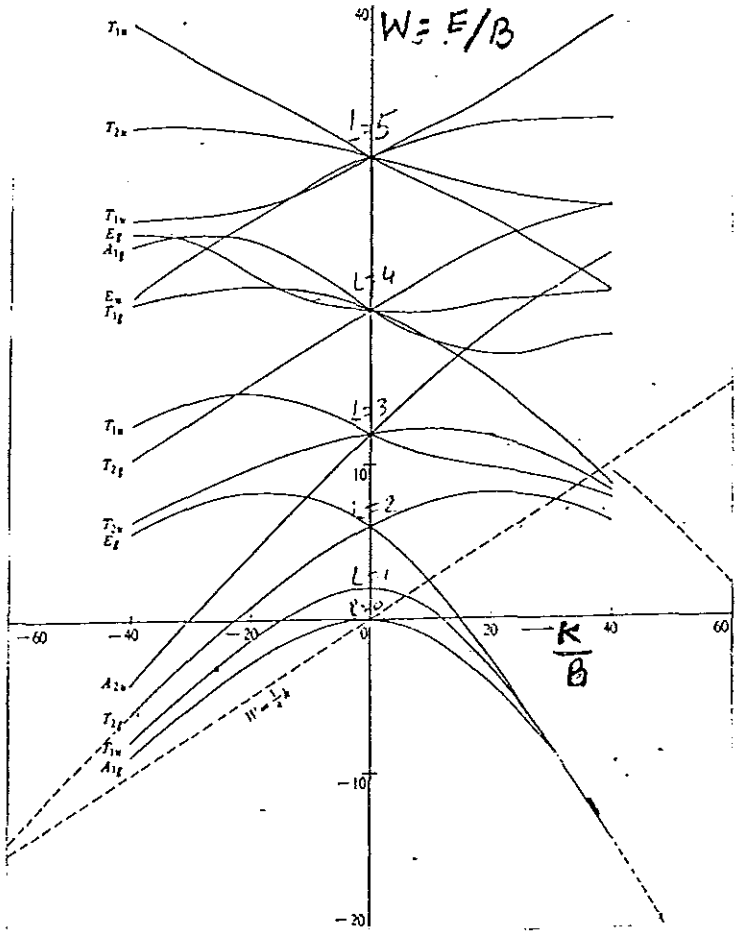

Fig.5 Energy levels as a function of k/B[1]

These results give us the values of the rotational energy eigenvalues for the few low lying energy levels, upto $\ell = 5$ and for the range of the potential parameter K, between -40 and 40 in units of the rotational constant B. It is evident from Fig.5 that as the values of k/B increase the rotation of the molecule is highly hindered and for the value W = E/B to the left of the line $W = \frac{1}{4}k$, which is set of saddle points, the molecule is rotating. But to the right of this line since the gap between the energy levels is wide we can consider the motion of the molecule to be oscillation rather than rotation.

A rather detailed and improved calculation with a better accuracy for the energy levels was computed by Sauer (1966)[5] for a wide range of the potential parameter k between -100 and 100. Sauer showed that the further we expand our angular momentum eigenfunctions, which are the spherical harmonics, of the series of the respective representation of the O_h group, the better will be the accuracy of the energy values. Infact the energy values obtained by Devonshire are found to be in good agreement with those obtained by Sauer for low lying energy levels. The discripancy between the two calculations are highly pronounced for larger values of the potential parameter k.

2.2 Comparison of Devonshire Model With Experimental Investigations

The validity of the obtained rotational energies and in general that of the Devonshire model is evaluated by comparing the experimentally obtained results with those calculated by the model.

All the experimental data[6,7,8] used for testing the reality of the model are taken from the measurements of the heat capacity and thermal expansion conducted on inert gas matrices containing different concentrations of diatomic impurities at low temperatures, between 2k and 12k. These solid solutions include Ar-co, Ar-N_2, Kr-co, Kr-N_2 and many others. These measurements are considered due to the fact that at low temperatures rotating impurities can introduce an appreciable, sometimes dominant contribution to the heat capacity and thermal expansion of solid solutions of inert gases and hence can be used to investigate the dynamics of the impurity molecule in these matrices.

The contribution of the rotating impurity molecules to the heat capacity and to the linear expansion coefficient is the main indicators in analyzing the rotational motion of the molecules.

The heat capacity of a given solid solution can be written as

$$C = C_o + \Delta C \tag{2.16}$$

where C_o is the heat capacity of the pure inert gas matrix under consideration and ΔC is the excess heat capacity which is given by

$$\Delta C = \Delta C_{rot} + \Delta C_{mass} \tag{2.17}$$

where ΔC_{rot} the contricution of the impurity molecules due their rotational motion and ΔC_{mass} is the contribution to the heat capacity that arises whenever the molar volumes of the host atoms and the molecule does not coincide which is related to the difference in mass and force constants

of the solution components. However, one can consider such systems where the molar volumes of the components coincide such as Kr - N_2 and Kr - Co. In such cases we have

$$C = C_o + \Delta C_{rot}$$

or dropping the subscript

$$C = C_o + \Delta C \tag{2.18}$$

If the free energy of the solid solution is expressed as the sum of the free energies of the lattice of the matrix and that associated with the system of discrete impurity levels, the heat capacity of the solid solutions is computed from the Devonshire spectrum by using the relation[9]

$$C = \frac{1}{kT^2} [\langle E^2 \rangle - \langle E \rangle^2] \tag{2.19}$$

where $\langle E \rangle$ is the average energy, k the Boltzmann constant and T is the temperature. And the averaging is performed over the impurity molecule energy spectrum

$$\langle \cdots\cdots \rangle = \frac{\sum_i (\cdots\cdots) g_i e^{-E_i/kT}}{\sum_i g_i e^{-E_i/kT}} \tag{2.20}$$

where E_i is the energy of the i^{th} level and g_i is the degree of its degeneracy. So that comparison between calculated and experimental values of the excess heat capacity indicates the degree of accuracy of the computed energy spectrum.

In a similar way for discrete energy spectrum the excess coefficient of linear expansion of a solid solution could be computed by[6]

$$\Delta\alpha = \frac{\chi}{\Omega kT^2}\left[\langle E^2\gamma\rangle - \langle E\gamma\rangle\langle E\rangle\right] \qquad (2.21)$$

where Ω and χ are the molar volume and the compressibility of the solution and the Gruneisen parameter for the i-th level of the impurity is defined by

$$\gamma_i = -\frac{V}{E_i}\frac{\partial E_i}{\partial k}\frac{\partial k}{\partial V} \qquad (2.22)$$

where K is the parameter defining the depth of the potential barrier and V is the volume of the system. By the help the above relation the coefficient of thermal expansion could be obtained from the enrgy spectrum of the model. A more reliable information about the model could be obtained by comparing the calculated and experimental value of the coefficient of linear expansion (CLE) since it involves both the rotational energy values and the potential field strength parameter or rather on the magnitude of the hindering crystal field.

The results of experimental investigations on both heat capacity and thermal expansion exhibited that Devonshire model is incapable of explaining the obtained experimental dependencies[6,7,9][10]. The failure of Devonshire model to interpret experimental results even qualitatively is observed for many systems studied.

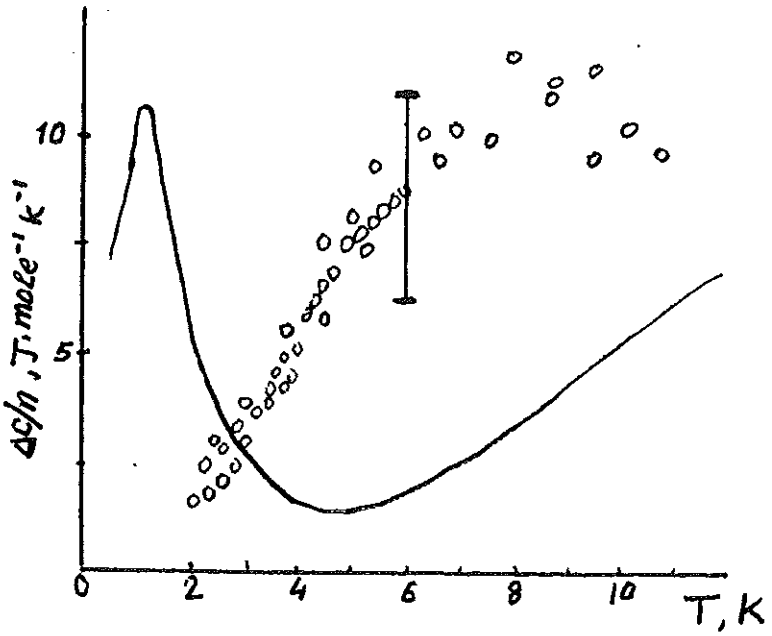

Fig.6 Excess heat capacity of solid solutions Kr-Co per 1 mole of impurity. O-experiment, ... calculation of DM. [From Ref.6]

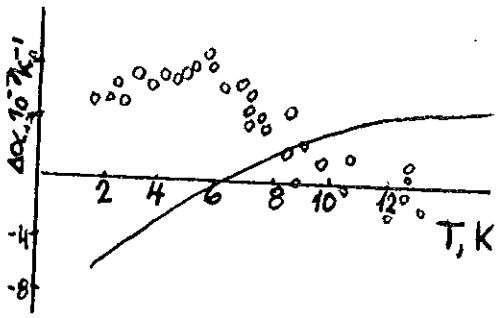

Fig.7 Experiment and computed temeprature dependence of the excess coefficients of linear expansion for Ar-Co. O-expt and solid curve calculation of Devonshire model[6]

Fig.6 for instance show that the heat capacity behaviour for Kr-Co system is quite different from that predicted by Devonshire model. In addition Fig.7, a comparison of the excess CLE computed by the model and the experimental values clearly shows the weakness of the model. In Devonshire model negative values of CLE are predicted below 6K whereas the experimental values in this region correspond to the maximum positive CLE values. Even in the region where the impurity effect is very small or negligble, the model predicts maximum effect.

Existing data on the low temperature heat capacity, thermal expansion and spectroscopy[11] of a molecular impurity in atomic cryocrystals exhibit unquestionably that the Devonshire model completely fails in interpreting the rotation of diatomic molecules in atomic inert gas matrices.

2.3 Shortcomings of Devonshire Model

The inadequency of Devonshire model to interpret experimental findings in mainly its neglect of possible lattice relaxation of the surrounding host atoms that result when the impurity molecule is placed in a crystal[7]. Devonshire calculated the energy spectrum by considering the crystal lattice to be rigid, thereby ignoring lattice vibrations and lattice distortions by the impurity. The model also does not take into account impurity-impurity interactions. As pointed by Kalnoi[12] the presence of impurities around an impurity imposes a distortion in the local vicinity of the chosen impurity, as a result of which additional splittings of the Devonshire spectrum will be observed.

Other observations[13] also show that the separation of the lattice motion and that of the molecule leads to a noticable descripancies between the calculated and experimental values regarding higher rotational states of the impurity molecule.

Moreover, the octahedral symmetry of the potential, which reflects the symmetry of the lattice may not be the same when the impurity is replaced due to the non-spherical shape of the impurity molecules and the anisotropy of the intermolecular interactions resulting in anisotropic nature of the relaxations of the surroundings of the molecules.

Based on these observations, the model must be modified by taking into consideration the major factors which are neglected. Such an attempt in extending the Devonshire model was done by Manz and Mirsky[14] latter called the Devonshire-Manz-Mirsky model which considers the influnce of lattice relaxations into a minimum energy configuration for a given impurity molecule configuration.

CHAPTER III

EXTENSION OF DEVONSHIRE MODEL. [DEVONSHIRE - MANZ - MIRSKY MODEL]

The neglect of lattice distortion being the main weak point of the Devonshire model, Manz and Mirsky studied the rotation of diatomic molecules in a crystal by considering the influnce of the relaxations of the lattice near the impurity molecule as well as the intermolecular interaction[14] in order to modify the Devonshire model.

The subsequent consequences of these relaxations on the rotational energy spectrum in general, and on the magnitude of the crystal field in particular is discussed. Although a rearrangement of the surrounding host atoms due to the rotating molecule is explained as a pseudoration of the relaxation region, they proposed that such a rearrangement took place much more rapidly than the molecular rotation and hence the octahedral symmetry of the crystal field will be restrored; thereby ruling out the possibility of lowering of the symmetry of the field.

3.1 The Geometry of Co Molecule in Argon Matrix

For demonstrating how a relaxation of a soft lattice and its pseudorotation result due to the rotation of an impurity molecule, we consider a typical example, the rotation of Co molecule in Argon matrix. The geometry of the Co molecule for a given orinetation and the corresponding lattice relaxations are studied by using force-field calculations[14].

A Co molecule is known to be ellipsoidal in shape and has a volume of $26.9\mathring{A}^3$. This molecule is fitted into a single vacancy substitutional site

provided by the volume of a single Ar atom in the crystal whose volume is 27.7Å^3.

The favourable orientation of the Co molecule in the vicinity of the distorted Ar lattice is such that the total interaction potential energy V will have its global minimum

$$V - V_o = \Delta V = \min \tag{3.1}$$

where V_o is a constant reference value defined conventionaly as the sum the interaction potential of the undistorted Ar atoms and that of the free Co molecule.

The total interaction potential[14,15] will consist the interamolecular potential V_{mol}, the interaction potential between all Ar atoms in the matrix V_{mat} and that of between the Co molecule and Ar atoms of the matrix V_{Ar-Co}. Hence we write the interaction potential as

$$V = V_{C-o} + V_{AT} + V_{mol-mat} \tag{3.2}$$

The interamolecular energy is expressed using Morse potential where the necessary parameters are taken from the gas-phase spectra and from solid state properties

$$V_{mol}(r-r_e) = D(e^{-2\beta(r-r_e)} - 2e^{-\beta(r-r_e)}) \tag{3.3}$$

where $r = |R_c - R_o|$ is the internuclear distance between the carbon and oxygen atom, $r_e = 1.283\text{Å}$ is the equilibrium moleculear gas phase distance,

D = 1083.22kJ/mol and $\beta = 2.2996\text{Å}^{-1}$. These parameters[16] are taken as to fit the spectroscopic vibrational frequency w = 2169.8cm^{-1}.

Using the atom-atom approximation, the interaction potential of the matrix and the interaction potential of the matrix and the molecule which consists of pair wise C-Ar and O-Ar atom-atom potentials are given respectively as

$$V_{mat} = \tfrac{1}{2} \sum_{i \neq j=1}^{n} V_{Ar\text{-}Ar}(R_{ij}) \tag{3.4}$$

$$V_{mat\text{-}mol} = \sum_{i=1}^{n} [V_{Ar\text{-}c}(R_{i\text{-}c}) + V_{Ar\text{-}Co}(R_{i\text{-}o})] \tag{3.5}$$

where the summations are carried over all the Ar atoms of the lattice located at a distance R_i, i = 1,2,...n and R_{ij}, $R_{i\text{-}c}$ and $R_{i\text{-}o}$ are distances from the i^{th} Ar atom to the j^{th} Ar atom, to the carbon and oxygen atom respectively.

The interaction potentials of Eqs.(3.4) and (3.5) are given by the (6 exp.) Buckingham[17] form as

$$V(R) = \frac{-A}{R^6} + B\, e^{-\alpha R} \tag{3.6}$$

where the numerical parameters A,B and α are chosen as to fit the known solid state properties.

The reference value V_o defined earlier is also given by

$$V_o = V_{mol}(0) + \tfrac{1}{2} \sum_{i \neq j=o}^{n} V_{Ar\text{-}Ar}(R_{ij}^{o}) \tag{3.7}$$

Using equations (3.2) to (3.7) and the condition for global minimum energy Eq.(3.1) could be written as

$$\Delta V = [V_{mol}(r-r_e)-V_{mol}(0)] + \tfrac{1}{2}\sum_{i\neq j=1}^{n}[V_{Ar-Ar}(R_{ij}) - V_{Ar-Ar}(R_{ij}^{o})]$$

$$+ \sum_{i=1}^{n}[V_{Ar-c}(R_{ic}) + V_{Ar-o}(R_{io}) - V_{Ar-Ar}(R_{io}^{o})] = \min \qquad (3.8)$$

The minimization procedure employed by Manz and Mirsky involves two steps using CYBER175 computer. First they[14] found the approximate minimum by varying the center of mass and orientation of Co molecule and in the second step the Ar matrix with the impurity is allowed to relax into minimum energy configuration by successively increasing the relaxed and undistorted sites.

Rather than the detailed minimization used it is the results obtained that is of great importance for our discussion here. It was obtained that the global minimum is always attained when the molecule is oriented along the (001) crystal axis. With respect to this energetically preferable orientation further minimization by considering the relaxation of the whole lattice show that the 8 nearest neighbour atoms in the polar configuration will be pushed away from the molecule by approximately 0.05Å from their original equilibrium position and the 4 nn atoms in the equatorial configuration are attracted by to the molecule by 0.06Å. Fig.8 shows such host atoms shift into new momentary equilibrium positions for different molecular orientations.

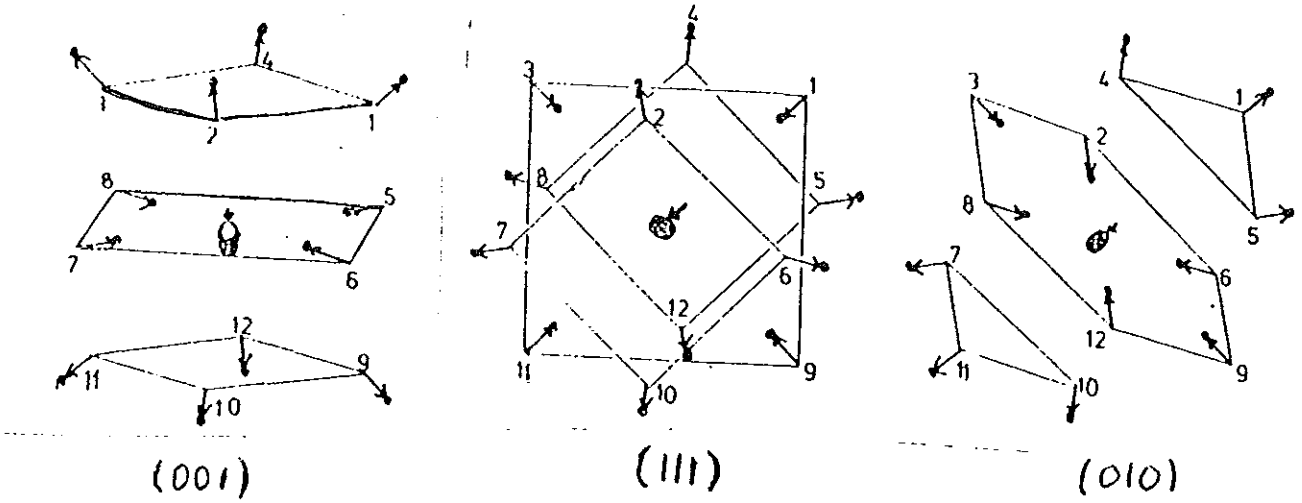

Fig.8 Shift of host atom due to a rotating molecule[13]

As a consequence, the first 12nn atoms or the first shell of Ar atoms relaxed into its optimal shape which is roughly ellipsoiddal. The major and minor axes devating by 0.06Å from the radius of the undistorted sphere of the first shell of the Argon atoms r = 3.756Å and the potential minimum being -0.16KJ/mol.[14].

Other shells distortions are not appericiable as the deviation of the atoms in these shells are of the order of 10^{-4} Å. So that their contribution to ΔV is completely negligble, as should be expected since the Co-Ar potential will be very small for distant shells.

The likely conclusion that could be drawn out of this is that the optimum configuration of the Co molecule in Ar matrix is determined by the molecular relaxation and the first shell atoms relaxations. This is in agreement with studies conducted using polyatomic molecules as impurity in matrices by Craig et al[18] and with other investigations[19,20].

3.2 Effects of Rotating Molecule Orientation and Cage Deformation

As a result of the crystal atoms relaxations into a momentary new equilibrium positions for a given molecular orientation, the rotating molecule always finds itself trapped in a cage which has different shape from the undistorted lattice spherical cage[13]. Whenever the lattice relaxations are faster than the rotation of the molecule, the shape of the distorted cage resenbles the shape of the rotating impurity molecule.

All the time as the rotating molecule changes its orientation the cage deformation too will follow the molecule and will be oriented along the molecular orientation. Fig.9 shows this rotation of the molecule trapped in pseudorotating cage.

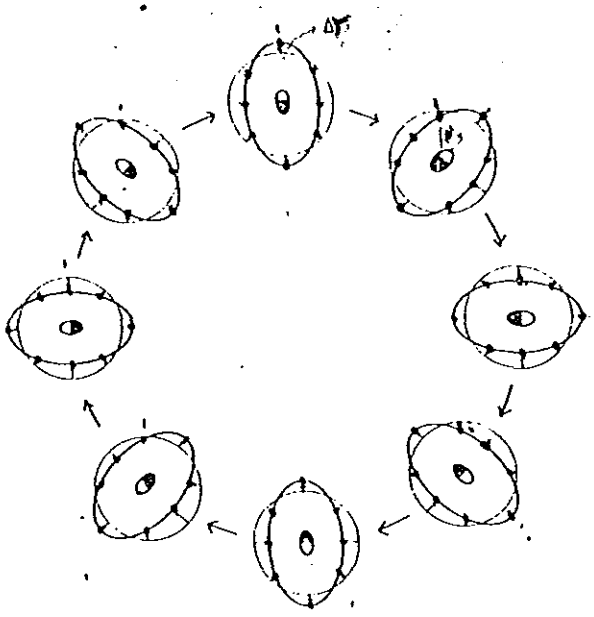

Fig.9 Rotating molecule trapped in synchronously rotating cage. The black-white ellipsoid represent the molecule, the black dots are the host nn atoms, heavy continuous lines the distorted cage and thin curves show the undistorted spherical cage[13]

We call such a cage pseudorotating since it is set up by cooperative small deviations of the nn host atoms and not by actual rotation of these atoms.

J. Manz[13] clearly formulated that due to the syncronous cage pseudorotating and molecular rotation two main effects are observed which influence the rotational energy spectra of the molecule in the host lattice. These are:

a) increase of moment of inertia of the rotating molecule

b) replacement of the Devonshire cell potential of the undistorted lattice by a new relaxed lattice potential.

These two effects deserve detail treatment and explanation for they are important points leading to the modification of the Devonshire model.

3.2a Effective Moment of Inertia of a Rotating Molecule

It is observed that the moment of inertia of a molecule rotating in a pseudorotating cage sometimes exceeds by 50% than that of the moment of inertia of the molecule in the gas phase. The considerable increase of inertia influences the rotational or liberational energy spectra of matrix isolated molecules.

Calculations based on lattice relaxations exhibit two effects which lead to an increase of the effective moment of inertia of the rotating molecule. The first one being the contribution of the effective rotation of the molecular center of mass around the center of interaction which is given by

$$\Delta I_{ci} = Ma^2 \tag{3.9}$$

where $a = |\vec{R}_{ci} - \vec{R}_{cm}|$ is the distance of the center of interaction from the center of mass and M is the mass of the molecule. This moment of inertia

is independent of the molecular orientation. If the rotating molecule is homonuclear $a = o$ and the contribution of ΔI_{ci} is zero.

The second contribution for an increase of inertia comes from the synchronously pseudorotating cage. The magnitude of this inertia could be estimated from the values obtained from lattice relaxations. As seen from Fig.9, when the guest molecule rotate through an angle θ between 0 and 2π, the equilibrium position of the neighbouring atom i oscillates around its undistorted lattice site according to a simple harmonic motion given by

$$\Delta r_i(\theta) \simeq \Delta r_i \sin(2\theta + \delta i) \tag{3.10}$$

Note that the factor 2 indicates the double speeded pseudorotation in comparison to the molecular rotation. The average kinetic energy of this pseudorotating cage is

$$T_{rot} \simeq \tfrac{1}{2} \sum_i M_i \overline{\Delta \dot{r}_i^2} \tag{3.11}$$

where the sum extends over all nn atoms.

If the moment of inertia due to the pseudorotating cage is ΔI_{cage}, then a molecule rotating with a frequency ω induces a pseudorotation of its cage with kinetic energy

$$T_{rot} = \tfrac{1}{2} \Delta I_{cage} \omega^2 \tag{3.12}$$

So using the above two equations, an estimate of the magnitude of ΔI_{cage} is computed by

$$\Delta I_{cage} \simeq 2 \sum_i M_i \Delta r_i^2 \qquad (3.13)$$

The total effective moment of inertia associated with the molecular rotation and pseudorotation is given by

$$I_{eff} = I_o + \Delta I_{ci} + \Delta I_{cage} \qquad (3.14)$$

For instance for Co molecule in Ar, Manz and Mirsky[14] found $a \simeq 0.25\text{Å}$, $\Delta r_i \simeq 0.06\text{Å}$ and hence $\Delta I_{ci} = 1.75$ AmuÅ^2, $\Delta I_{cage} \simeq 3.46$ AmuÅ^2. With the gas-phase molecular moment of inertia $I_o = 8.73$ AmuÅ^2, the total effective moment of inertia $I_{eff} \simeq 13.94$ AmuÅ^2 exceeds by 12% that the inertia in the gas phase of the molecule.

In Devonshire model the contributions ΔI_{ci} and ΔI_{cage} were neglected in calculating the rotational energy values, despite the fact this contribution is worth considering.

3.2b Effective Crystal Potential

Another aspect of DMM model consideration as a consequence of lattice relaxation and pseudorotation is the replacement of the Devonshire potential $\tilde{V}(\theta,\phi)$, Eq.(2.6), by an effective potential $\tilde{V}(\theta,\phi)$. Since the distance between the molecule and the nn atoms differ from that of the unrelaxed Devonshire lattice, the rotating molecule in a given (θ,ϕ) orientation faces a new renormalized crystal field in the relaxed lattice hence the corresponding interaction potential $\tilde{V}(\theta,\phi)$ will be different from that of the Devonshire cell potential.

Though the field is different, the DMM model assumes that the octahedral symmetry of the field will not change[13]. The main reason given for the restortation of the symmetry is since the relaxations of the atoms in the vicinity of the molecule takes place much faster than the molecule's rotation and the corresponding equivalent reorientations of the impurity will lead to equivalent geometrical distortion, and hence the field retains it original symmetry.

The new renormalized crystal field is given by

$$\tilde{V}(\theta,\phi) = \tilde{V}_o + \tilde{K}v(\theta,\phi) = \tilde{V}_D(\theta,\phi) \qquad (3.15)$$

where $Kv(\theta,\phi)$ is the Devonshire unrelaxed potential, $\tilde{V}_o$ is a constant and $\tilde{K}$ is the new renormalized potential barrier parameter. The constants $\tilde{V}_o$ and $\tilde{K}$ are the two adjustable parameters of the model.

The interaction potentials of the unrelaxed and relaxed lattice for Co in Ar are shown in Figs.10 and 11 respectively. Eventhough the approximately constant ellipsoidal shape of the cage may suggest a smooth variation between $V(\theta,\phi)$ and $\tilde{V}_D(\theta,\phi)$, the difference $V-\tilde{V}_D$ is not necessarly constant.

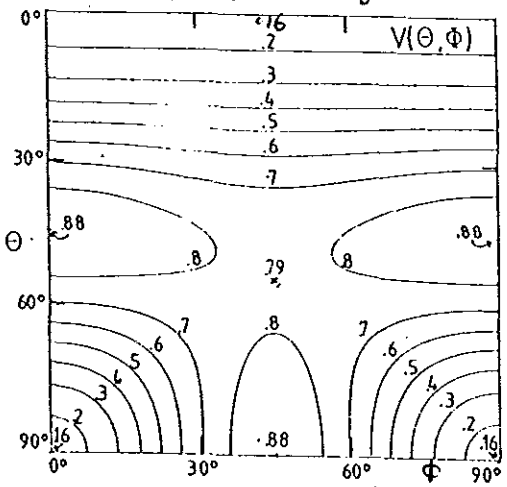

Fig.10 Potential energy $V(\theta,\phi)$ for Co in Ar[13]

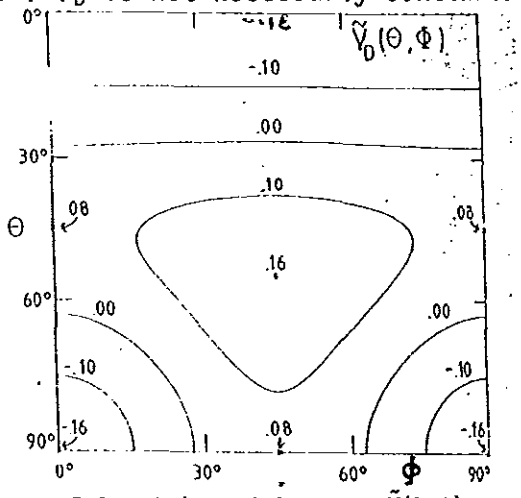

Fig.11 Relaxed potential energy $\tilde{V}(\theta,\phi)$ for Co in Ar[14]

For Co in Ar when the molecule is oriented in (001) direction the lattice relaxation result in decrease from $V(0°,0°)$ = 0.16KJ/mol(min) and $V(54.7°, 45°)$ = 0.79KJ/mol (max) to $\tilde{V}_D(0°,0°)$ = - 0.16KJ/mol(min) and $\tilde{V}_D(54.7°, 45°)$ = 0.16KJ/mol. It could be seen that the potential barrier has reduced from ΔV = 0.63KJ/mol to $\Delta \tilde{V}_D$ = 0.32KJ/mol which asserts the condition that the potential energy of the molecule should be minimum and the consideration a new potential to be reasonable.

The minimum and maximum values for $V(\theta,\phi)$ of Devonshire potential were given by -K and $^2/_3$ K (section 2.1), so that the minima and maxima of $\tilde{V}_D$ are obtained from

$$\tilde{V}_D(0°,0°) = \tilde{V}_o - \tilde{K}$$
$$\tilde{V}_D(54.7°, 45°) = \tilde{V}_o + \tfrac{2}{3}\tilde{K} \qquad (3.16)$$

Hence the parameters $\tilde{V}_o$ and $\tilde{K}$ for Co in Ar have the values 0.03KJ/mol and 0.19KJ/mol respectively so that the value $\Delta \tilde{V}_D$ = 0.32KJ/mol could be obtained.

Hence the effect of the relaxations and pseudorotation could be considered as a renormalization of the molecular rotation constant B through the increase of moment of inertia and the barrier parameter K due to the renormalized field.

Since the rotational constant B is inversly proportional to the moment of inertia, an increase in the moment of inertia yields a reduction of the rotational constant, i.e., the renormalized rotational constant

$$\tilde{B} = B\left(\frac{I_o}{I_{eff}}\right) \qquad (3.17)$$

and also the new barrier parameter is chosen as to given the appropriate $\tilde{V}_0(\theta,\phi)$.

Once the proper value of $\tilde{K}/\tilde{B}$ for a given system is known, the rotational energy values of the rotating molecule can readily be obtained from the Devonshire's spectrum. On the other hand if experimental results of the rotational energy values are known, one can determine the rotational constant and the barrier parameter by choosing the value of $\tilde{K}/\tilde{B}$ which fits best the experimental curve.

3.3 Test for the Validity of DMM Model

The results of many experimental investigations on the measurements of heat capacity and coefficient of thermal expansion on inert gas materices at low temperatures has been used to interpret these results in the framework of DMM model by varying the two adjustable parameters $\tilde{K}$ and $\tilde{B}$. The systems used for these studies include Ar and Kr matrices containing Nitrogen and Co molecules of different concentrations in the temperature range 2K-12K[6,21,22].

The experimental curves of the excess heat capacity obtained for various matrices are compared with those calculated by the model (cf. Fig.12a,b,c,d). The comparison reveals that the experimental results of the excess heat capacity could be better described by the DMM model than those predicted by the Devonshire model. This good agreement between the computed and the experimental values is achieved for the respective chosen parameters of $\tilde{K}/\tilde{B}$.

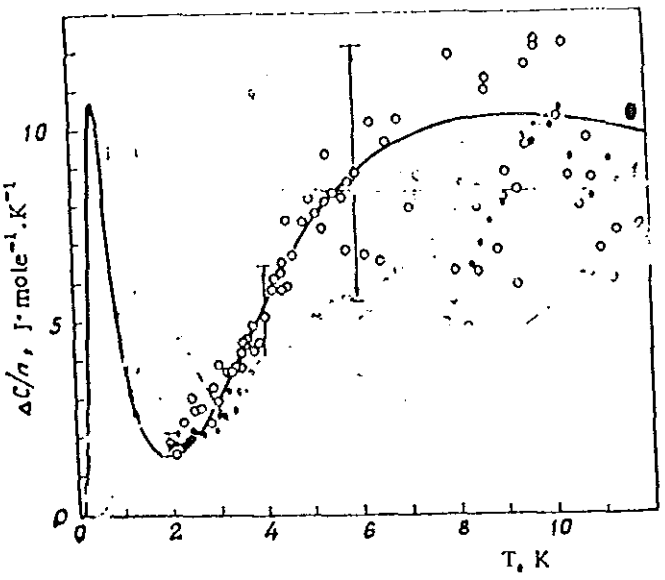

Fig.12a Excess heat capacity of the solid solution Kr-Co. Experiment. 0 for 0.95%, for 1.87% Co calculated: solid curve $\tilde{K}/\tilde{B} = 20$ and $\tilde{B}/B = 2.5$[6]

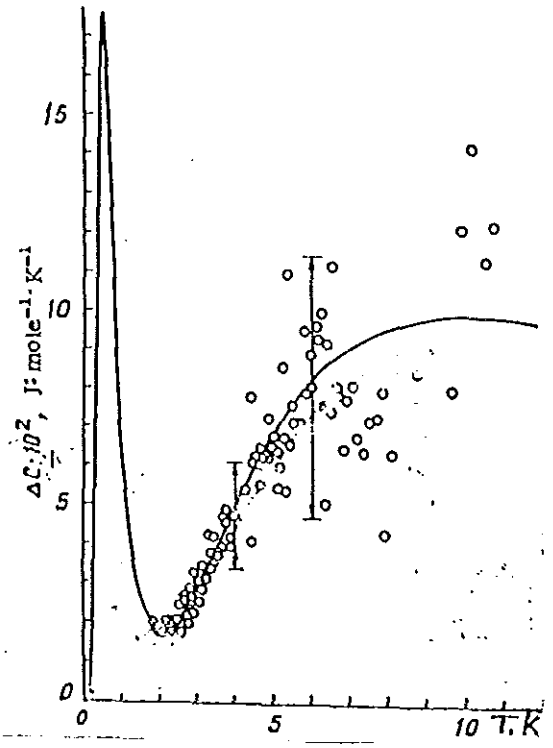

Fig.12b Kr.-$^{15}N_2$

Experiment: 0 for 1.02% $^{15}N_2$

Calculated: solid curve for $\tilde{K}/\tilde{B} = 16$, $\tilde{B}/B = 2$[6]

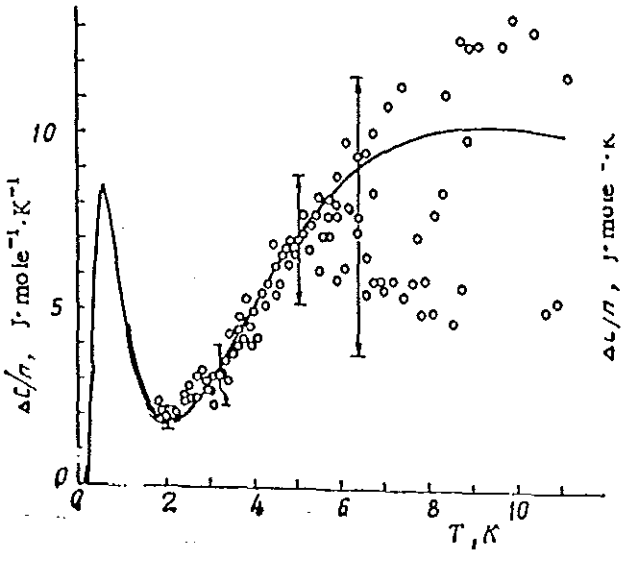

Fig.12c Kr-$^{14}N_2$

Experiment: 0 for 0.95 mole % of $^{14}N_2$

Calculated: Solid curve[6]

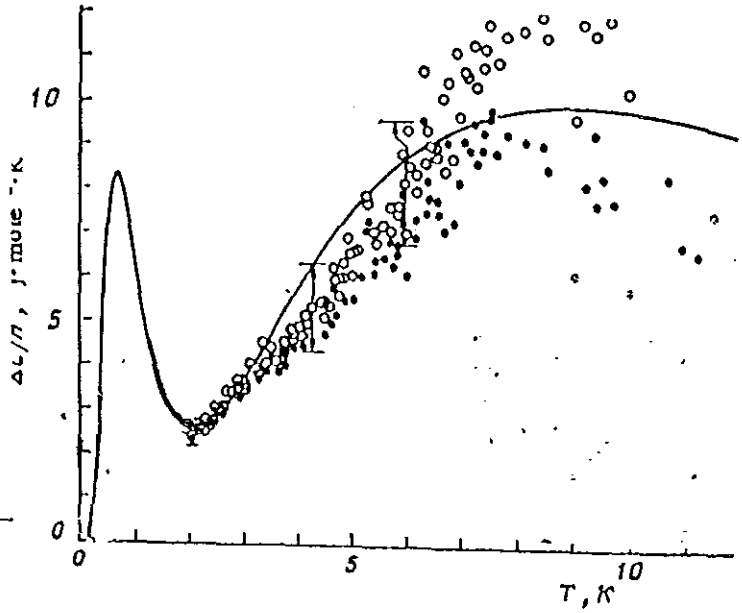

Fig.12d Ar-$^{14}N_2$

Experiment: 0 for 1.06 mole% N_2

Calculated: Solid curve[6]

However results of experimental investigations of the excess thermal expansion of the above solid solutions depart considerably from the curves calculated by the model. (cf. Fig.13a,b,c). In particular Fig.13b and 13c show substantial difference completely unpredictable by the model. Since the coefficient of expansion involves not only the energy spectrum like heat capacity, but also on the change of the energy spectrum with respect to the potential barrier, it is much more sensitive to the degree of inaccuracy of the model.

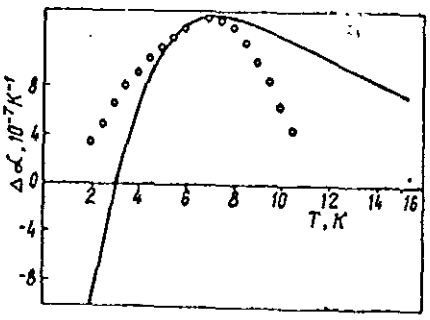

Fig.13a $Ar-^{14}N_2$

Experiment: 0 for 0.5 mole % N_2

Calculation: Solid curve[6]

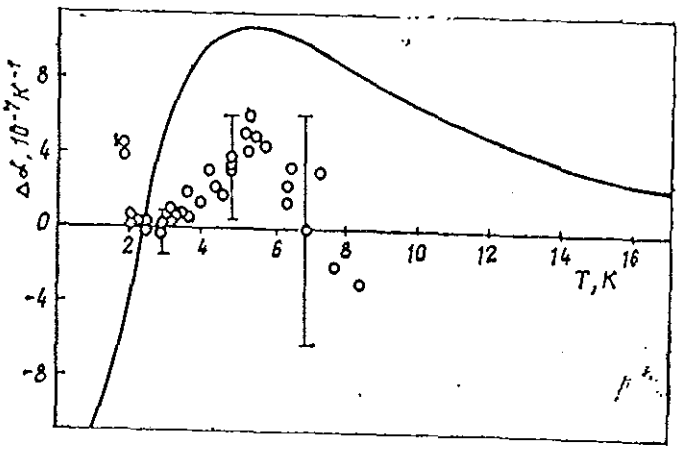

Fig.13b

Experiment: 0

Calculation: Solid curve[6]

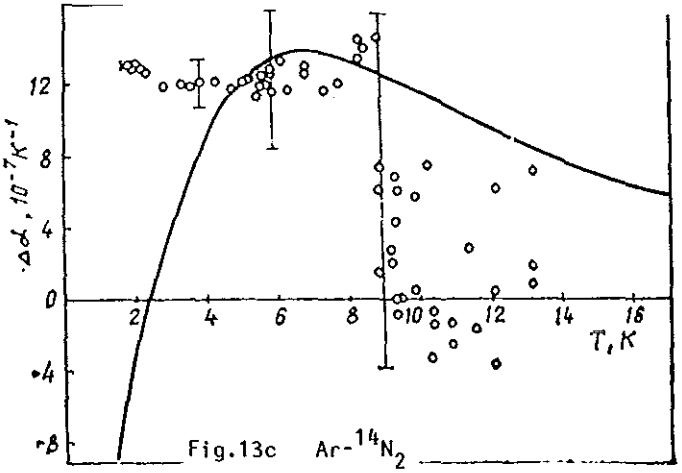

Fig.13c $Ar-^{14}N_2$

Experiment: Circles

Calculated: Solid curve

3.4 The Need for an Alternate Model

It has been shown that experimental results on heat capacity that could not be interpreted by Devonshire model are better understood in the framework of the DMM model. This should not obscure the fact that best agreements between computed curves and experimental values are attained by choosing the $\tilde{K}/\tilde{B}$ values as to get the best possible fit. Even with such freedom of choices of the values of the parameters, the model does not accurately describe the experimental results in the whole range considered. The DMM model predicts a peak values for heat capacity calculations below 2K which need to be further investigated. The model is also unable to explain the experimental dependencies obtained for thermal expansion measurements for the solid solutions considered.

These shortcomings suggest the need to have a model that can describe the rotation of diatomic molecules in inert gas crystals. This may be achieved by calculating the energy spectrum of a rotating molecule in a crystal field whose symmetry is lower than octahedral group. The choice of a lower symmetry could be understood from geometric consideration such that the relaxed lattice may not have the same symmetry as the undistorted lattice symmetry.

Furthermore, since the lattice distortion is caused by the impurity molecule, employing the rotational spectrum of the molecule calculated in the undistorted lattice symmetry can not serve as a proper description for the rotation of the molecule. As to the question, to what lower symmetry the distortion lead we proposed a strongest distortion, a tetrahedral one, than the suggested trigonal and tetragonal symmetry[9], for these only give splitting of the lowest lying excited rotational energy levels T_{1u} and E_g.

CHAPTER IV

ROTATION OF DIATOMIC MOLECULES IN FIELDS OF TETRAHEDRAL SYMMETRY

4.1 Reduction of Symmetry Group

The possible lattice distortion due to the rotation of diatomic molecules in crystal may result in the reduction of the symmetry group of the crystal to a lower subgroup.

The symmetry of a slightly distorted octahedron may be reduced to lower groups such as trigonal and tetragonal point groups[23]. For instance, if the octahedron of atoms are distorted by an elongation along one of the C_3 axes (Fig.1) the rotational symmetry will be reduced to a trigonal D_3 group. Similarly a distortion along the C_4 axes may lead us to a tetragonal D_{4h} group; in which case four of the six atoms which form the octahedron are now placed at the corner of a square and the remaining two will be located above or below this plane of this square.

As far as the octahedral symmetry levels are concerned the two fold degenerate levels split into two nondegenerate levels under the influence of additional tetragonal field and the three-fold levels will aplit into one nondegenerate and one two fold degenerate level under the influence of both tetragonal and trigonal fields. The scheme of splitting of the O_h levels under additional field is shown below:

$A_1 \rightarrow A_1$	$A_{1g} \rightarrow A_{1g}$
$A_2 \rightarrow A_2$	$A_{2g} \rightarrow A_{1g}$
$E \rightarrow E$	$E_g \rightarrow A_{1g} + B_{1g}$
$T_1 \rightarrow A_2 + E$	$T_{1g} \rightarrow A_{2g} + E_g$
$T_2 \rightarrow A_1 + E$	$T_{2g} \rightarrow B_{2g} + E_g$

Table IX. Splittings of the O_h levels under (a) trigonal (b) tetragonal distortion

The trigonal and tetragonal fields are of interest for study of the rotation of molecules inside a crystal fields. Instead we chose a lower symmetry of the O_h group, the tetrahedral T_d group, which result in a more stronger distortion of the lattice (octahedron of atoms) than the above two. We expected the result for tetragonal and trigonal symmetry should lie between those of the O_h and the tetrahedral groups. The configuration of the lattice atoms providing the crystal field and the symmetry elements of the T_d group are given in sect.1.1.

Since the lattice atoms are considered to provide the crystal potential field possessing the symmetry of their configuration, so a reduction in symmetry leads us to change the form of the potential function to that having the new symmetry.

Ballhausen[24] has shown that we can take over all the theory developed for the O_h point group and apply it for the tetrahedral point group. Furthermore, by noting the correspondence between the representations of O_h and T_d groups, the rotation of diatomic molecules in a crystal field having tetrahedral symmetry could be investigated. Therefore, hereafter we followed Devonshire's procedure to determine the form of the eigenfunctions and the rotational energy levels.

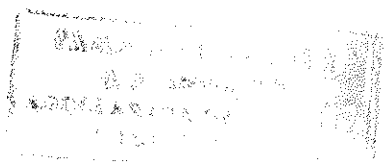

4.2 Rotational Wavefunctions and Energy Levels

We are now concerned in solving the Schrödinger equation (Eq.2.7) of a diatomic molecule rotating in a field $V(\theta,\phi)$ possessing tetrahedral symmetry.

$$\frac{1}{\sin\theta}\frac{\partial}{\partial\theta}\left(\sin\theta\frac{\partial\psi}{\partial\theta}\right)+\frac{1}{\sin^2\theta}\frac{\partial^2\psi}{\partial\phi^2}+\frac{8\pi^2 I}{h^2}[E-V(\theta,\phi)]\psi=0$$

This equation is invariant under the operations of the T_d group.

Bethe[3] has proved that the only spherical harmonics of degree less than four and possessing the required tetrahedral symmetry is

$$P_3^2(\cos\theta)\sin 2\phi \tag{4.1}$$

Hence, we used the simplest form of the potential energy

$$V(\theta,\phi) = -K P_3^2(\cos\theta)\sin 2\phi \tag{4.2}$$

which could be written as

$$V(\theta,\phi) = -30K\sin^2\theta\cos\theta\sin\phi\cos\phi \tag{4.3}$$

Referred to the axes through the midpoints of opposite sides of the fundamental tetrahedron (i.e., a tetrahedron of points of a unit sphere where $V(\theta,\phi)$ has min values), see Fig.14, the potential has minimum value of $-\frac{10}{\sqrt{3}}K$ at each vertex and has a maximum value $\frac{10}{\sqrt{3}}K$ at each vertex of the conjugate tetrahedron.

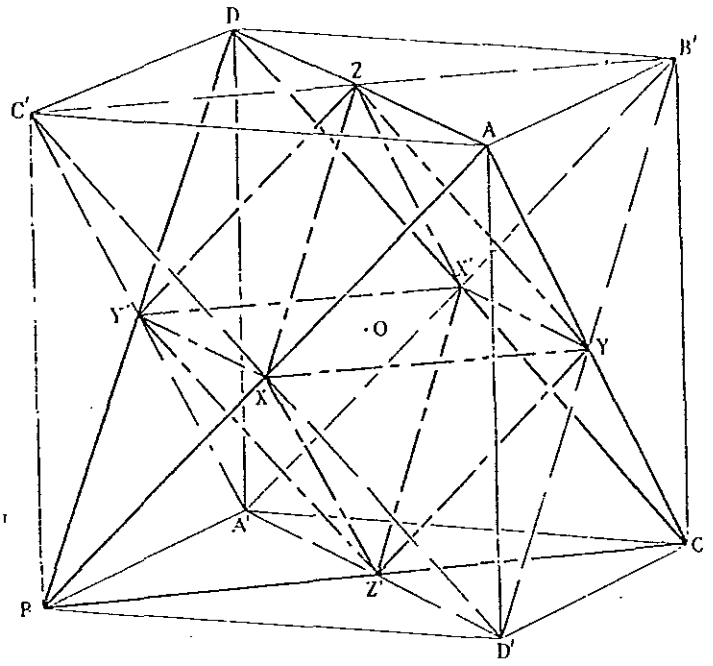

Fig.14 Fundamental (ABCD) and conjugate (A'B'C'D') tetrahedral with the fundamental octahedron of the O_h group.

Since the Schrodinger equation is invariant under T_d operations, its solutions i.e., the rotational wavefunctions must belong to the representations of the T_d group; A_1, A_2, E, T_1 and T_2 as given in Sect.1.1, Tab.II.

For the case of free rotation $V(\theta,\phi) = 0$, the solutions are all spherical harmonics of degree ℓ having energy $E = \ell(\ell + 1)$ in units of the rotational constant B. This degeneracy will be partially removed under the influence of the tetrahedral field and the solutions split up as shown in Table X. This scheme of splitting of the rotational energy levels under tetrahedral field is obtained by employing the method used in Sec.1.3.

ℓ		ℓ	
0	. . . A_1	7	. . . $A_1 + E + 2T_1 + 2T_2$
1	. . . T_2	8	. . . $A_1 + 2E + 2T_1 + 2T_2$
2	. . . $E + T_2$	9	. . . $A_1 + A_2 + E + 2T_1 + 3T_2$
3	. . . $A_1 + T_1 + T_2$	10	. . . $A_1 + A_2 + 2E + 2T_1 + 3T_2$
4	. . . $A_1 + E + T_1 + T_2$	11	. . . $A_1 + 2E + 3T_1 + 3T_2$
5	. . . $E + T_1 + 2T_2$	12	. . . $2A_1 + A_2 + 2E + 3T_1 + 3T_2$
6	. . . $A_1 + A_2 + E + T_1 + T_2$		

Table X. Splitting of levels undet tetrahedral field

As the solutions of the Schrodinger equation are series of spherical harmonics, the different types of linear combinations of these harmonics are determined by inspecting the correspondence that exists between the representations of the octahedral group and the T_d group. For instance, since the O_h group has the complete symmetry of the tetrahedral T_d group, the expansion in splherical harmonics of a wave function which is of a type A_1 of T_d group will consists of terms of functions of the type A_{1g} and A_{2u} under the operations of the corresponding O_h group.

The correspondence between the representation of the O_h and T_d representation is listed below:

T_d	O_h
A_1	A_{1g} and A_{2u}
A_2	A_{1u} and A_{2g}
E	E_{1u} and E_{1g}
T_1	T_{1g} and T_{2u}
T_2	T_{1u} and T_{2g}

Table XI. Correspondence between T_d and O_h groups.

A comparison between the relationships of the symmetry types of T_d and O_h symmetries with the series of expansion of representation of O_h given in Sect.2.1, Tab.VII yields the following types of series of expansion of spherical harmonics for the different representations of the T_d group.

T_d representation	Series
A_1	$a_o^o + a_2^o\ p_2^o + a_4^o\ p_4^o + a_4^4\ p_4^4 \cos 4\phi + \ldots$
	$+ b_3^2\ p_3^2 \sin 2 + b_5^2\ p_5^2 \sin 2\phi + \ldots$
E	$a_2^2\ p_2^2 \cos 2\phi + a_4^2\ p_4^2 \cos 2\phi + a_6^2\ p_6^2 \cos 2\phi + a_6^6 p_6^6 + \ldots$
	$+ b_5^4 p_5^4 \sin 4\phi + b_7^4\ p_7^4 \sin 4\phi + \ldots$
T_1	$a_3^2\ p_3^2 \cos 2\phi + a_5^2\ p_5^2 \cos 2\phi + \ldots$
	$+ b_4^4\ p_4^4 \sin 4\phi + b_6^4\ p_6^4 \sin 4\phi + \ldots$
T_2	$a_1^o\ p_1^o + a_3^o\ p_3^o + a_5^o\ p_5^o + a_5^4\ p_5^4 \cos 4\phi + \ldots$
	$+ b_2^2\ p_2^2 \sin 2\phi + b_4^2\ p_4^2 \sin 2\phi + \ldots$

Table XII. Types of solutions of the Schrödinger equation and their representations

Once the series of spherical harmonics for a given type of representation is known, we can compute the rotational energy levels as a function of the potential barrier parameter K for aparticular form of the potential energy. Unlike the Devonshire potential, the change of the sign of K results

only in the interchange of the fundamental and the conjugate tetrahedrons[25]. Also the energy levels plotted as function of K will be symmetrical about the line K = 0, so we considered only positive values of K in calculating the energy values.

Upon substitution of the eigenfunction and the form of the potential energy function Eq.(4.2) in the Schrödinger equation, we need to know the expansions of the products

$$P_3^2(\cos\theta)\sin 2\theta \;.\; P_\ell^m(\cos\theta)\cos m\phi$$

or

$$P_3^2(\cos\theta)\sin 2\theta \;.\; P_\ell^m(\cos\theta)\sin m\phi \qquad (4.4)$$

in terms of spherical harmonics. These product could be simplified by the use of the recurrence relations of the associated legendre polynomials. Here we shall present only the results obtained which are useful for the computations. These are given in series of P_s^{m-2} and P_s^{m+2} as follows:

$$P_3^2 . P_\ell^m = \frac{15(\ell-m+5)(\ell-m+4)(\ell-m+3)(\ell-m+2)(\ell-m+1)}{(2\ell+1)(2\ell+3)(2\ell+5)} P_{\ell+3}^{m-2}$$

$$- \frac{15(\ell-m+3)(\ell-m+2)(\ell-m+1)(\ell+m)(\ell+3m-2)}{(2\ell-1)(2\ell+1)(2\ell+5)} P_{\ell+1}^{m-2}$$

$$- \frac{15(\ell-m+1)(\ell+m)(\ell+m-1)(\ell+m-2)(\ell-3m+3)}{(2\ell-3)(2\ell+1)(2\ell+3)} P_{\ell-1}^{m-2}$$

$$+ \frac{15(\ell+m)(\ell+m-1)(\ell+m-2)(\ell+m-3)(\ell+m-4)}{(2\ell-3)(2\ell-1)(2\ell+1)} P_{\ell-3}^{m-2}$$

$$P_3^2 \cdot P_\ell^m = \frac{15(\ell - m + 1)}{(2\ell+1)(2\ell+3)(2\ell+5)} P_{\ell+3}^{m+2} - \frac{15(\ell-3m-2)}{(2\ell-1)(2\ell+1)(2\ell+5)} P_{\ell+1}^{m+2}$$

$$- \frac{15(\ell+3m+3)}{(2\ell-3)(2\ell+1)(2\ell+3)} P_{\ell-1}^{m+2} + \frac{15(\ell+m)}{(2\ell-3)(2\ell-1)(2\ell+1)} P_{\ell-3}^{m+2}$$

Our equation to be solved could be written as

$$\frac{1}{\sin\theta} \frac{\partial}{\partial\theta}(\sin\theta \frac{\partial\psi}{\partial\theta}) + \frac{1}{\sin^2\theta} \frac{\partial^2\psi}{\partial\phi^2} + [W + K P_3^2(\cos\theta)\cos 2\phi]\psi = 0 \qquad (4.5)$$

where $W = \frac{E}{B}$, $k = \frac{K}{B}$ and $B = \frac{h^2}{8\pi^2 I}$

It was shown in Tab.X how the solution of the Schrodinger equation split for a given energy level ℓ. We then take the series for the different representations and substitute for ψ in Eq.(4.5). Using the recurrence relations, every term is expressed as a sum of spherical harmonics and equating the coefficients of each separate harmonics to zero yields a set of linear equation. The condition that should be satisfied by these set of equations to be consistent gives us an infinite determinantal equation for W corresponding to each different type of solution in Tab.XII. An approximate solution of this infinite determinant is obtained by taking the first few rows and columns and solve the eigenvalues using computer, in which we took 9x9 determinant for each series.

Since the determinant is arranged as to contain W = E/B along its diagonal element, the eigenvalues obtained will be the values of the few low-lying energy level.

The computed values W for few arbitrarly chosen values of the field strength parameter K are given in Tab.XIII. A plot of the energy levels as a function of K/B which enables us to compare the variation of the energy values of the levels with respect to the field strength is given in Fig.15.

Symmetry Species	W = E/B										
	$\frac{K}{B}=0$	$\frac{K}{B}=1$	$\frac{K}{B}=2$	$\frac{K}{B}=3$	$\frac{K}{B}=4$	$\frac{K}{B}=5$	$\frac{K}{B}=6$	$\frac{K}{B}=8$	$\frac{K}{B}=10$	$\frac{K}{B}=15$	$\frac{K}{B}=20$
A_1	0	-0.7	-2.61	-6.42	-8.69	-12.35	-16.28	-24.59	-33.31	-56.23	-80.09
T_2	2	0.93	-1.57	-5.83	-8.32	-12.07	-16.14	-24.53	-33.29	-56.22	-80.09
E	6	5.84	5.34	4.13	3.31	1.62	-0.13	-4.82	-10.46	-27.11	-45.87
T_2	6	6.01	5.77	4.52	3.86	1.65	0.3	-4.54	-10.29	-27.07	-45.86
T_1	12	11.57	10.42	8.36	6.7	5.3	1.86	-3.72	-9.86	-26.97	-45.83
A_1	12	11.85	11.48	10.9	10.53	10	9.24	7.44	5.01	-4.12	-16.94
T_2	12	12.44	13.37	14.46	14	13.7	12.41	10.06	7.19	-2.98	-16.49
T_2	20	19.78	19.23	19	18.44	18.9	17.51	15.12	11.64	0.61	-12.89
E	20	19.65	19.23	18.8	17.36	16.60	15.06	12.57	9.75	0.11	-13.02
T_1	20	20.19	20.44	20.78	20.57	20.25	19.26	16.58	12.96	1.37	-12.59
A_1	20	20.63	22.22	24.94	26.31	28.35	29.43	29.64	27.67	21.23	14.33
T_2	30	29.71	29.22	29.08	27.5	28.6	25.79	24.2	22.31	16.38	8.99
T_1	30	29.96	29.85	29.8	26.69	28.9	29.79	29.88	24.41	23.01	12.81
E	30	29.85	29.61	30.6	28.46	26.9	26.66	24.39	21.88	15.42	18.15
T_2	30	30.28	31.13	33.4	30.8	32.29	35.3	33.3	34.33	27.94	18.15

Table XIII Energy values for different K/B values

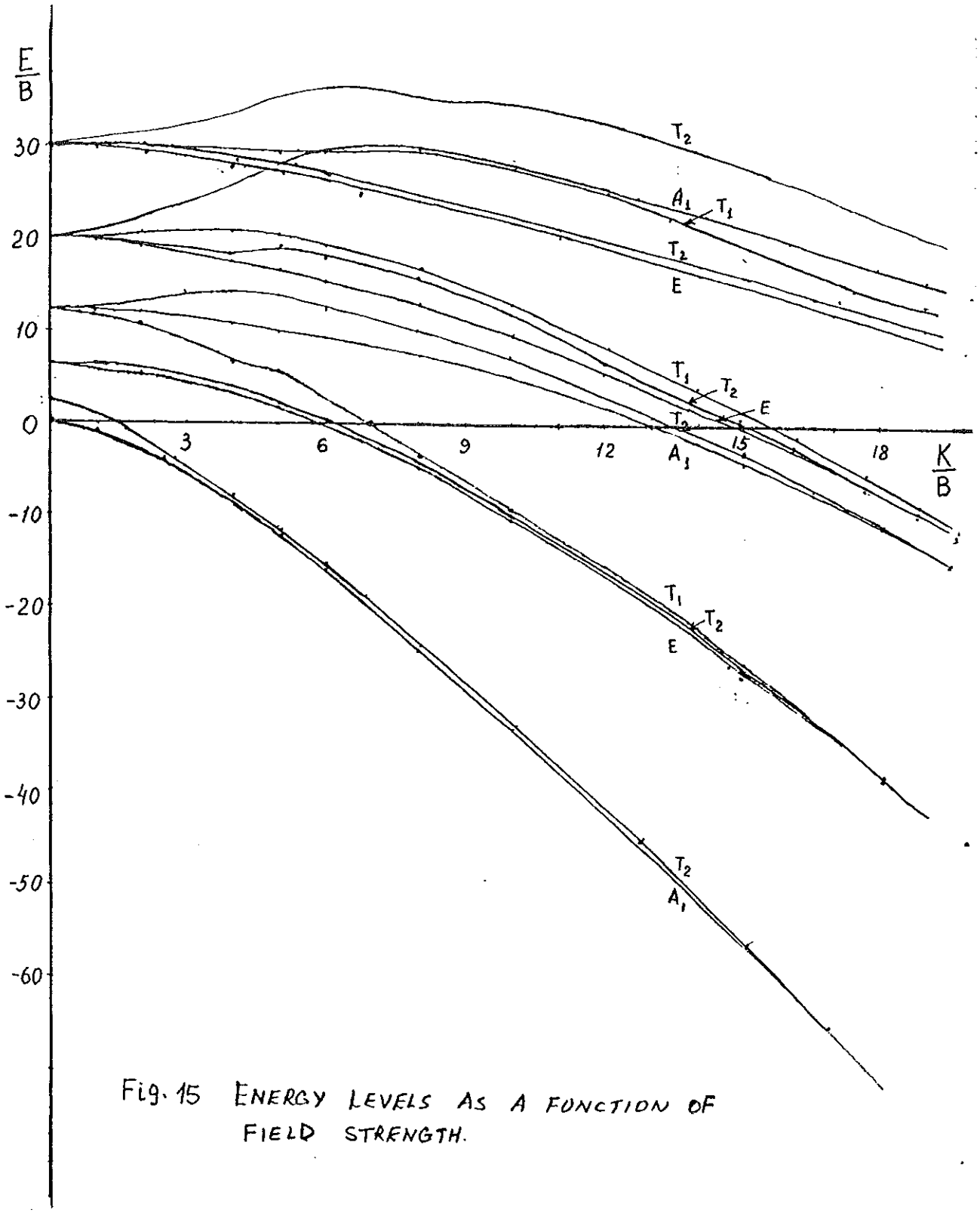

Fig. 15 ENERGY LEVELS AS A FUNCTION OF FIELD STRENGTH.

4.3 Comparison Between Calculated and Experimental Data for Heat Capacity of Co in Ar Matrix.

In order to analyze the applicability of the proposed local distortion of the symmetry of the crystal field from octahedral to a tetrahedral one, we made a comparison b/n experimental data[26] and the present calculated values. We used the experimental data obtained from heat capacity measurement in the temperature range from 0.5K to 10K in Co-Ar crystal system. The impurity concentrations considered are 0.07, 0.12 and 0.26 mole %. These data show a wide scattering in the temp range 5K-10K and only approximate values are taken.

From the calculated energy spectrum, the corresponding heat capacity values for a particular temperature are obtained from the relation

$$\Delta C = \frac{n}{KT^2} \left[\langle E^2 \rangle - \langle E \rangle^2 \right]$$

where the average energy

$$\langle E \rangle = \frac{\Sigma E_i g_i e^{-\frac{E_i}{kT}}}{\Sigma g_i e^{-\frac{E_i}{kT}}}$$

and E_i is the energy of the i^{th} level of the impurity molecule, g_i is its degeneracy and n is the impurity concentration in mole %. From the above relation, the contribution of the impurity molecule to the heat capacity of crystal system, i.e., ΔC is calculated for the temperature between 0.5-10K in step 0.5K using computer for different values of K.

The results of heat capacity calculations are compiled in Tab.XIV(a)-(f) for values of the hindering potential parameter $\frac{K}{B}$ = 1,2,3,4 and 5. The rotational constant 2.77°K for Co molecule is used.

The temperature dependence of the heat capacity calculated from the energy spectrum of tetrahedral field for Co-Ar system under consideration for different values of the field strength parameter K are plotted together with experimentally obtained values, in Figs.(16)-(18).

$\frac{K}{B} = 1$; B = 2.77K						$\frac{K}{B} = 2$; B = 2.77K					
E_i	Representation	g	E,Jx10^{-23}	T(°K)	$\frac{\Delta C}{n}$ (J mole^{-1}K^{-1})	E_i	Representation	g	E,Jx10^{-23}	T(°K)	$\frac{\Delta C}{n}$ J mole^{-1}K^{-1}
E_o	A_1	1	0	0.5	0.25	E_o	A_1	1	0	0.5	2.58
E_1	T_2	3	6.18	1	5.28	E_1	T_2	3	2.86	1	8.47
E_2	E	2	24.83	1.5	8.45	E_2	E	2	21.88	1.5	6.44
E_3	T_2	3	25.6	2	7.86	E_3	T_2	3	23.21	2	4.17
E_4	T_1	3	46.87	2.5	6.71	E_4	T_1	3	36.09	2.5	2.9
E_5	A_1	1	47.94	3	6.08	E_5	A_1	1	39.02	3	2.38
E_6	T_2	3	50.19	3.5	5.93	E_6	T_2	3	44.26	3.5	2.37
E_7	T_2	3	78.23	4	6.06	E_7	T_2	3	60.5	4	2.67
E_8	E	2	77.73	4.5	6.31	E_8	E	2	60.5	4.5	3.15
E_9	T_1	3	79.79	5	6.59	E_9	T_1	3	63.84	5	3.72
E_{10}	A_1	1	81.48	5.5	6.8	E_{10}	A_1	1	68.77	5.5	4.31
E_{11}	T_2	3	116.1	6	7.1	E_{11}	T_2	3	88.16	6	4.89
E_{12}	T_1	3	117.1	6.5	7.3	E_{12}	T_1	3	90.21	6.5	5.43
E_{13}	E	2	116.7	7	7.5	E_{13}	E	2	89.24	7	5.92
				7.5	7.6					7.5	6.36
				8	7.78					8	6.74
				8.5	7.89					8.5	7.06
				9	7.99					9	7.33
				9.5	8.06					9.5	7.55
				10	8.12					10	7.72

Table XIV. (a) – (f) Calculated excess heat capacity from the tetrahedral field spectrum.

$\frac{K}{B} = 3$; B = 2.77K

E_i	Representation	g	$E, Jx10^{-23}$	T(°K)	$\frac{\Delta C}{n}$ ($J\,mole^{-1}K^{-1}$)
E_o	A_1	1	0	0.5	8.12
E_1	T_2	3	2.26	1	5.16
E_2	E	2	40.34	1.5	2.46
E_3	T_2	3	41.83	2	1.36
E_4	T_1	3	56.51	2.5	0.86
E_5	A_1	1	66.27	3	0.64
E_6	T_2	3	79.84	3.5	0.61
E_7	T_2	3	97.2	4	0.77
E_8	E	2	96.43	4.5	1
E_9	T_1	3	103.3	5	1.81
E_{10}	A_1	1	120	5.5	2.3
E_{11}	T_2	3	135.74	6	2.9
E_{12}	T_1	3	138.5	6.5	3.5
E_{13}	E	2	141.5	7	3.87
				7.5	4.07
				8	4.6
				8.5	5.2
				9	5.7
				9.5	6.2
				10	6.7

Table XIV (c)

$\frac{K}{B} = 4$; B = 2.77K

E_i	Representation	g	$E, Jx10^{-23}$	T(°K)	$\frac{\Delta C}{n}$ $J\,mole^{-1}K^{-1}$
E_o	A_1	1	0	0.5	6.9
E_1	T_2	3	5.4	1	2.1
E_2	E	2	175.2	1.5	0.9
E_3	T_2	3	183	2	0.5
E_4	T_1	3	224.7	2.5	0.3
E_5	A_1	1	280.6	3	0.2
E_6	T_2	3	331.3	3.5	0.2
E_7	T_2	3	395.5	4	0.3
E_8	E	2	380.3	4.5	0.45
E_9	T_1	3	427.2	5	0.7
E_{10}	A_1	1	511	5.5	1.04
E_{11}	T_2	3	528.4	6	1.44
E_{12}	T_1	3	516.6	6.5	1.9
E_{13}	E	2	542.4	7	2.4
				7.5	3
				8	3.5
				8.5	4.07
				9	4.6
				9.5	5.2
				10	5.7

Table XIV (d)

$\frac{K}{B} = 5$; B = 2.77K

E_i	Representation	g	$E, Jx10^{-23}$	T(°K)	$\frac{\Delta C}{n}$ ($J\,mole^{-1}K^{-1}$)
E_o	A_1	1	0	0.5	4.6
E_1	T_2	3	1.06	1	1.18
E_2	E	2	53.3	1.5	0.49
E_3	T_2	3	53.48	2	0.26
E_4	T_1	3	67.42	2.5	0.16
E_5	A_1	1	85.37	3	0.11
E_6	T_2	3	99.5	3.5	0.1
E_7	T_2	3	119.3	4	0.13
E_8	E	2	110.6	4.5	0.21
E_9	T_1	3	124.5	5	0.34
E_{10}	A_1	1	155.4	5.5	0.55
E_{11}	T_2	3	156.4	6	0.81
E_{12}	T_1	3	157.5	6.5	1.1
E_{13}	E	2	150	7	1.5
				7.5	1.92
				8	2.37
				8.5	2.83
				9	3.32
				9.5	3.81
				10	4.3

Table XIV (e)

$\frac{K}{B} = 2$; B = 1.5K

E_i	Representation	g	$E, Jx10^{-23}$	T(°K)	$\frac{\Delta C}{n}$ $J\,mole^{-1}K^{-1}$
E_o	A_1	1	0	0.5	8.23
E_1	T_2	3	1.55	1	4.8
E_2	E	2	11.92	1.5	2.66
E_3	T_2	3	12.57	2	2.4
E_4	T_1	3	19.54	2.5	3.2
E_5	A_1	1	21.13	3	4.26
E_6	T_2	3	23.97	3.5	5.3
E_7	T_2	3	32.75	4	6.3
E_8	E	2	32.75	4.5	7.1
E_9	T_1	3	34.57	5	7.7
E_{10}	A_1	1	37.24	5.5	8.2
E_{11}	T_2	3	47.74	6	8.6
E_{12}	T_1	3	48.8	6.5	9
E_{13}	E	2	48.32	7	9.1
				7.5	9.17
				8	9.19
				8.5	9.15
				9	9.05
				9.5	8.9
				10	8.7

Table XIV (f)

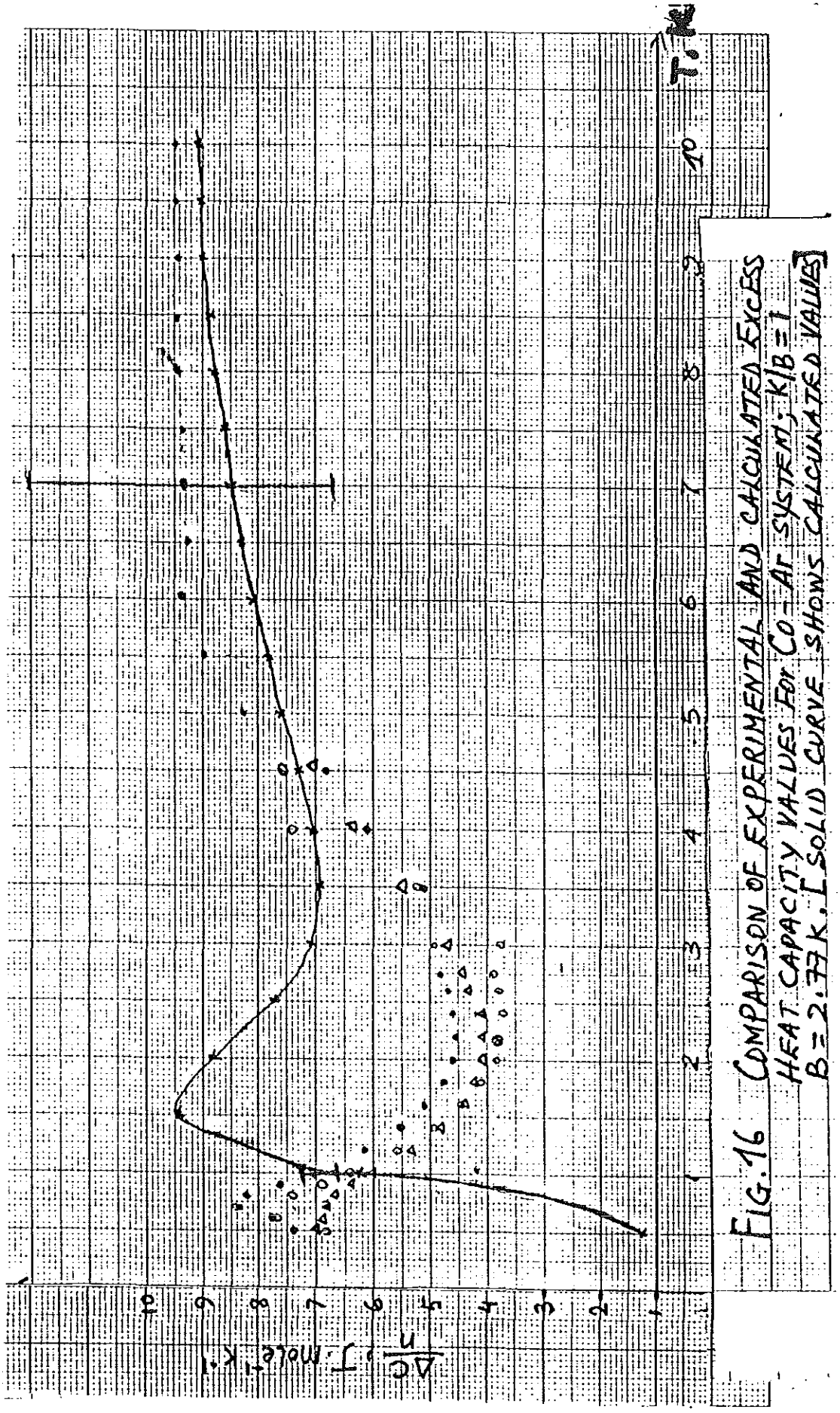

FIG. 16 COMPARISON OF EXPERIMENTAL AND CALCULATED EXCESS HEAT CAPACITY VALUES FOR C_0=Ar SYSTEM; K/B=1 B=2.77 K. [SOLID CURVE SHOWS CALCULATED VALUES]

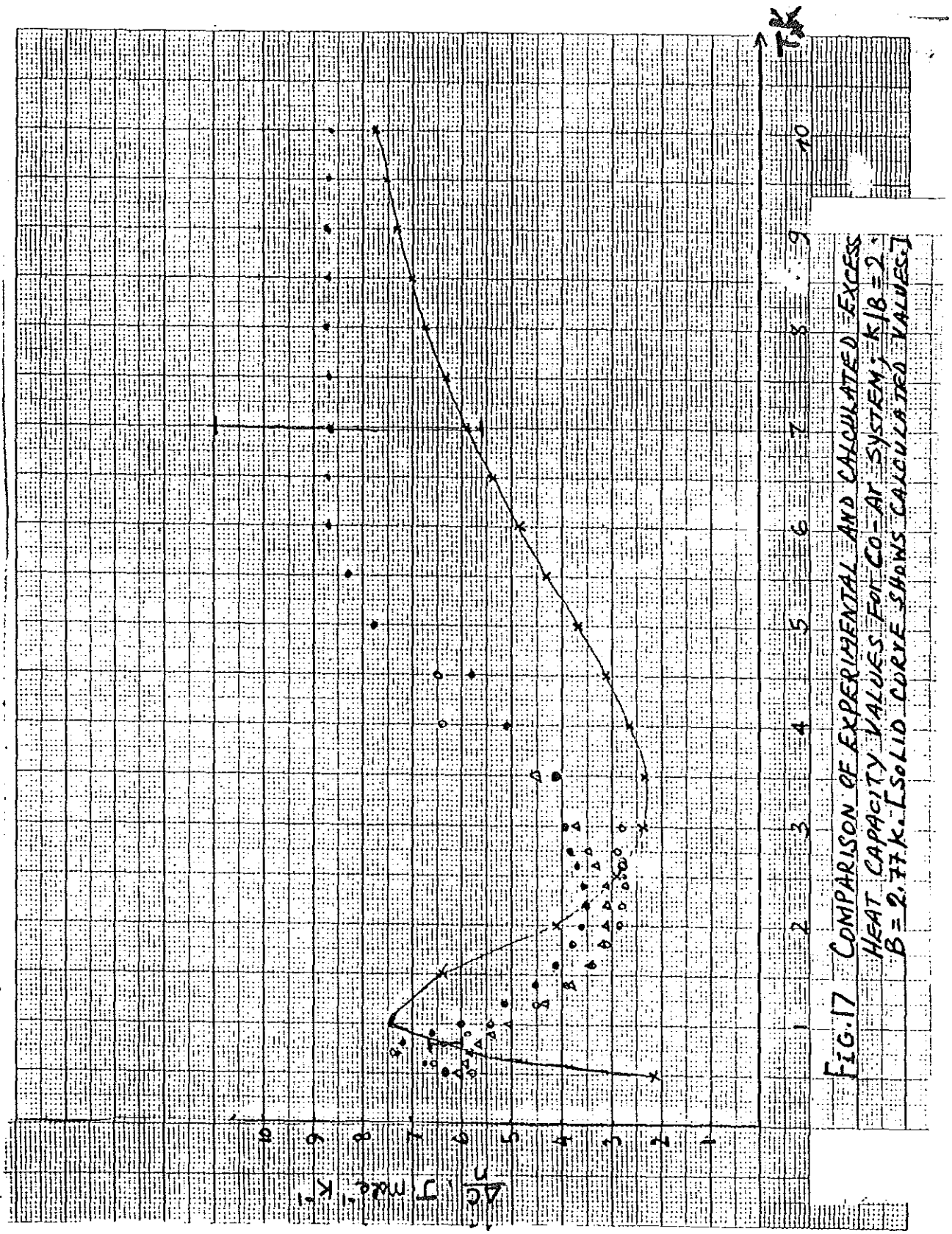

FIG. 17 COMPARISON OF EXPERIMENTAL AND CALCULATED EXCESS HEAT CAPACITY VALUES FOR CO-Ar SYSTEM; K/B = 2.77 K. [SOLID CURVE SHOWS CALCULATED VALUES.]

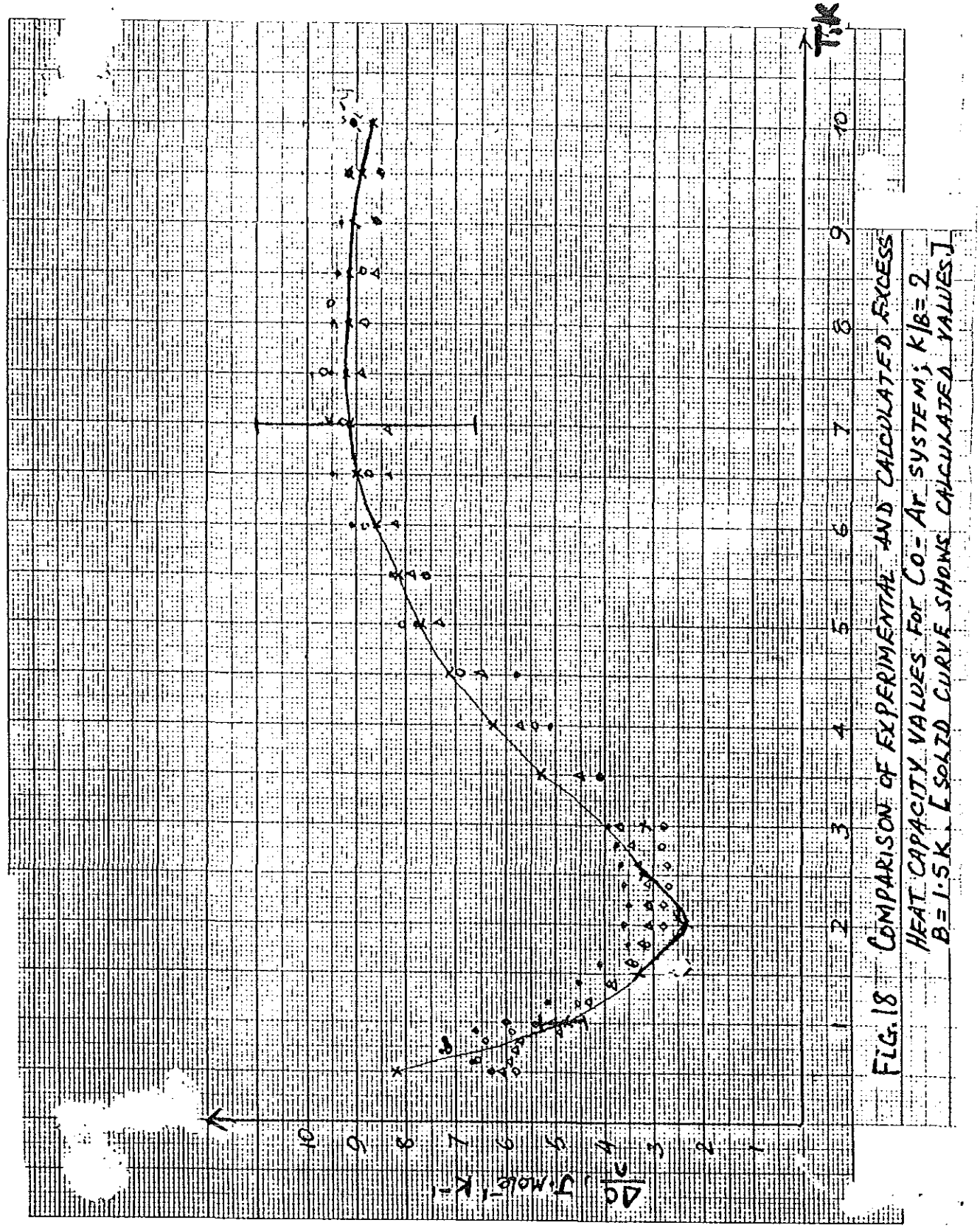

FIG. 18 COMPARISON OF EXPERIMENTAL AND CALCULATED EXCESS HEAT CAPACITY VALUES FOR Co-Ar SYSTEM; K/B = 2. B = 1.5 K. [SOLID CURVE SHOWS CALCULATED VALUES]

FIG. 19(a) COMPARISON OF EXPERIMENTAL AND CALCULATED EXCESS HEAT CAPACITY VALUES FOR K/B = 3, 4, 5. [SOLID CURVE SHOWS CALCULATED VALUES]

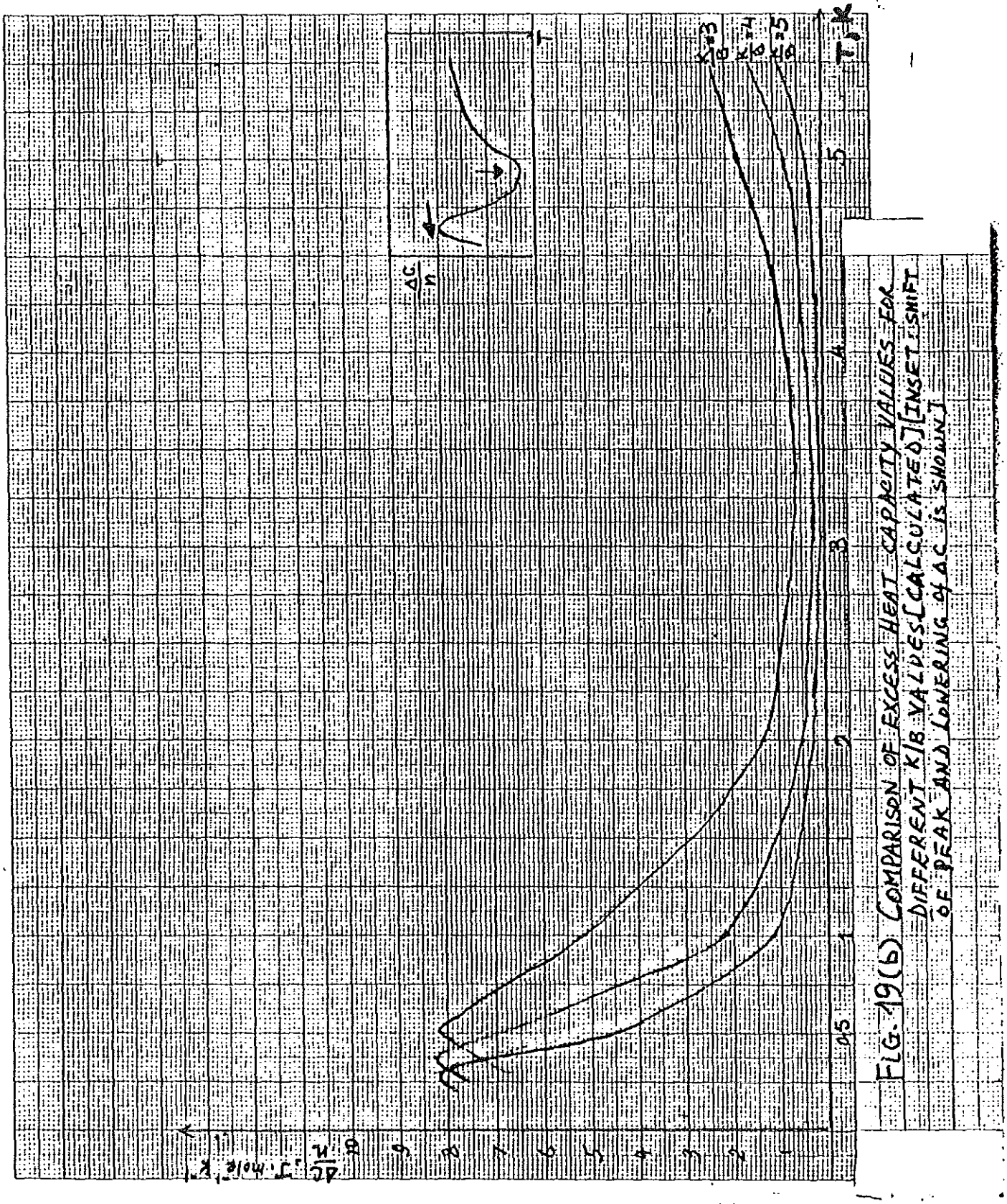

FIG. 19(b) COMPARISON OF EXCESS HEAT CAPACITY VALUES FOR DIFFERENT K/B VALUES [CALCULATED] [INSET: SHIFT OF PEAK AND LOWERING OF ΔC IS SHOWN]

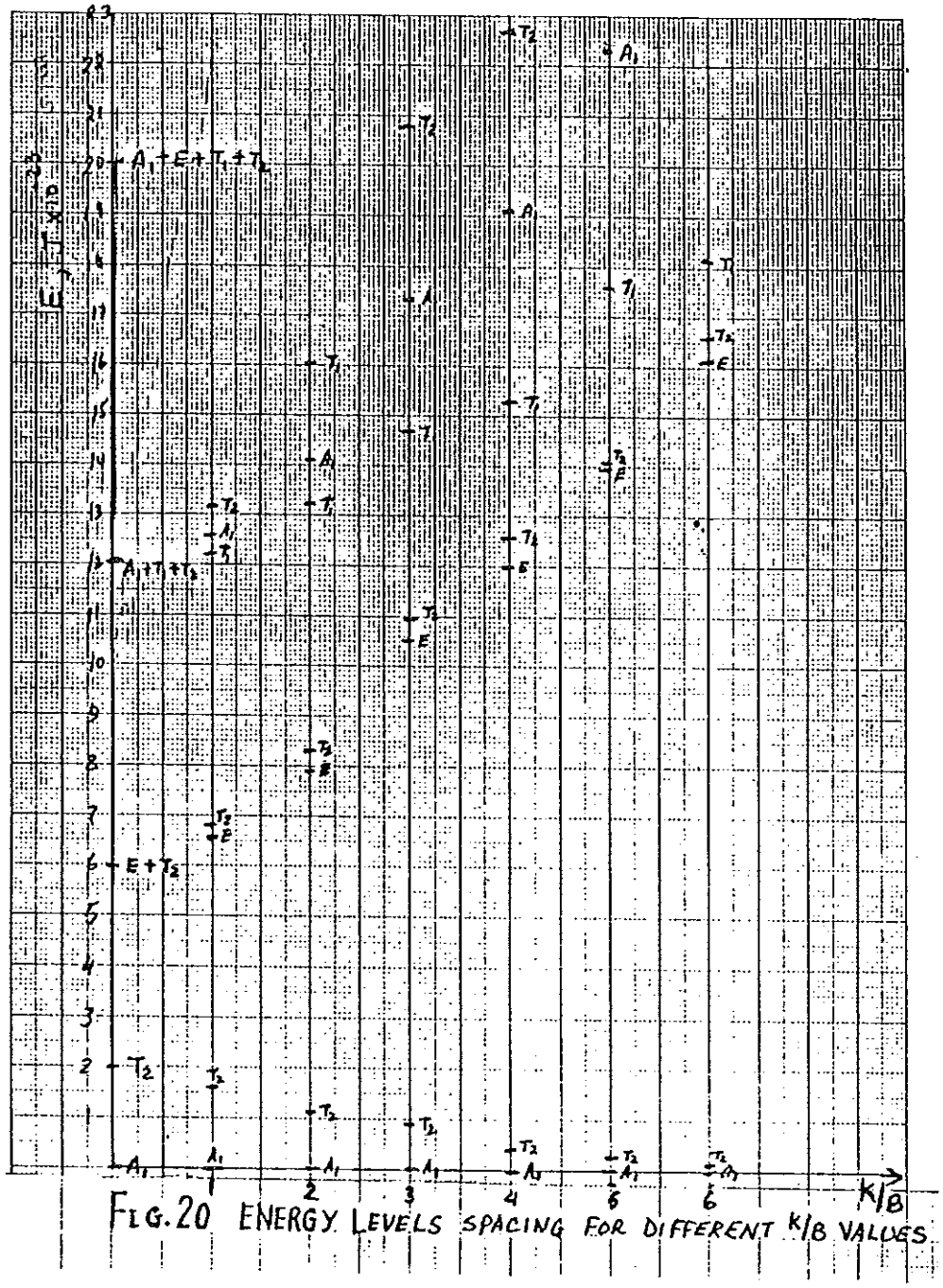

FIG. 20 ENERGY LEVELS SPACING FOR DIFFERENT K/B VALUES

Results of Comparison

The DMM model gives a good interpretation for experimental heat capactiy measurement by arbitrarly varying the two adjustable parameters of the theory the potential barrier parameter $\tilde{K}/K$ and the effective rotational constant $\tilde{B}/B$[13]. Unlike the DMM model, the results of calculation using tetrahedral field spectrum showed that a definite value of the potential barrier K could be known for a given system in order to explain the hindered rotation of molecules in inert gas in the whole temperature range under consideration.

In our case a good qualitative agreement between the experimental and calculated curves is obtained for the barrier parameter $\frac{K}{B} = 2$ (Fig.18). Peak values of excess heat capacity observed experimentally for the different concentration around 0.7K is also predicted by our calculation at 0.5K. Minimum heat capacity contribution by the impurities in both experimental and our calculation lies in the same temperature range 1.5K - 3K.

For the values of the barrier parameter $\frac{K}{B} < 2$, the obtained dependence could not explain experimental results, but rather they are closer to the free rotor spectrum which gives high heat capacity anomalies in the range 1K-2K; as an illustration the result for $\frac{K}{B} = 1$ is given in Fig.16.

Higher values of the potential barrier K/B, i.e., for more stronger field, the computed heat capacity values have no agreement with the experimental data as shown in Fig.19(a). Eventhough the heat capacity dependence for these higher values of K/B does not describe the experimental investigations, their pattern exhibit that the heat capacity anomalies are

observed to shift towards the lower temperature range and give much lower heat capacity values as the field strength increase. (See Fig.19(b)). Such situation is to be expected since when the field strength increases, as a result of the tetrahedral symmetry spectrum, the ground state (A_1) and the first excited state (T_2) are closer and hence their contribution to heat capacity of the matrix is considerable at very low temperature, $T < 0.5K$. At the same time the spacing between the first excited level and higher excited levels increases with the increase of the barrier parameter K/B and their contribution to heat capacity is very little. So in general we obtain very low heat capacity values (Fig.20). This is also evident from the point of view that when the spacing or energy gap between the excited levels increase the probability of the higher states to be occupied by the impurity molecules will be very small and their contribution to the heat capacity due to rotational excitation will be minimum. The higher excited levels occupation is more probable when the temperature increase sufficiently and enable the molecules to gain enough energy kT necessary to overcome the energy gap to be excited to higher levels.

Furthermore, as a consequence of the lowering of the local crystal field symmetry to a tetrahedral, we did not obtain highly degenerate levels in the lowest energy region, as is the case in DMM model. [Compare $A_1 + T_2$ and $A_{1g} + T_{1u} + T_{2g}$ levels in Figs.15 and 5 respectively]. Some studies propose that DMM model weakness i.e. its perdiction of a very high anomaly for $T < 2K$ could be improved if additional splittings of the lowest T_{1u} level is considered which could be attributed to lattice deformation in the vicinity of the impurity molecules. But instead of dealing on further splittings of one or two levels it is more reasonable to

assume the lattice distortion to lower the symmetry of the local crystal field, as in our case, in which not only the splitting of T_{1u} is achieved but also other levels giving comparatively better results for heat capacity anomalies.

Our calculated heat capacity results for T > 5K should have approached the theoretically predicted rotational heat capacity value $C_{rot} \approx 8.31J$ but we obtained a bit higher value 9.1J (see Fig.18).

A considerable quantitative agreement between experimental and calculated value could be obtained if interactions between the lattice atoms and the rotating molecule is taken into account. For instnace when the rotational constant of Co molecule B = 2.77°K is reduced to B = 1.5K (Fig.18), a much better agreement is achieved.

CHAPTER V

CONCLUSION

There are large number of works devoted to understand the rotation of impurity molecules dynamics and spectrum in a crystal field since the first mathematical description of the problem was formulated by L. Pauling (1930). A general model that explain the hindered rotation for wide range of energies and rotational quantum numbers does not yet exist.

The solutions of the Schrödinger equation for diatomic molecules rotating in an octahedral symmetry crystal field (a more accurate representation of the field in solids), the Devonshire model, which gives the rotational energies as a function of the field strength is reviewed. Though this model is unsuccessful in interpreting experimental results of heat capacity and thermal expansion measurements in inert gas matrices at low temperatures [0.5 - 12K] taking into account the crystal lattice to be rigid, the idea of using the principles of group theory in order to simplify the complication of solving the Schrödinger equation is found to be relevant.

The modified Devonshire model, DMM model, which takes into account the interaction between the rotational motion of impurity molecules and lattice vibrations, retaining the octahedral symmetry of the local crystal field, by renormalizing the rotational constant of the molecule and the magnitude of the crystal field is discussed in Chapter 3. This model suggests that a rotating impurity molecule always finds itself trapped in a pseudorotating cage. According to the two effects of this synchronously

rotating cage considered in DMM model, i.e., minimization of the molecule-crystal interaction potential and an increase in effective moment of inertia. The model employes two adjustable parameters; the reduced barrier and rotational constants for describing experimental heat capacity and thermal expansion observations at low temperatures in inert gas matrices with diatomic molecules as impurities. Though it describes the experimental results better than the Devonshire model, it was suggested that appreciable agreement both qualitatively and quantitatively could be achieved by considering the splitting of the low lying energy levels. But on the other hand the splitting of the low-lying levels gives an indication for the distortion of the octahedral symmetry to a lower summetry since these levels are more sensitive to change symmetry of the crystal field than the higher levels (compare Fig.15 and Fig.5).

Furthermore, taking into account the evidences in literature for the possibility of the distortion of the symmetry of the local crystal field around the impurity, we proposed to investigate the rotation of diatomic molecules in a crystal field with symmetry lower than octahedral, the tetrahedral symmetry. To this end our work is brouhgt into line with that of the procedure employed by Devonshire by noticing the connection between the tetrahedral T_d and octahedral O_h point groups. Using the calculated energy spectrum for a diatomic molecule in tetrahedral crystal field, numerical calculations of heat capacity for Co-Ar system is done for some value of the crystal field strength in the range of temperature from o.5K - 10K.

It was found that experimental data for small concentrations ($\leq$ 0.26 mole %) of Co in Ar can be described qualitatively in the temperature

range 0.5 - 10K. A quantitative agreement could be reached for the whole temperature ranged considered only when lattice interaction is considered. We also obtained the parameters which characterize the hindered rotation of Co molecule in solid Ar matrix. As a result, the rotation of the molecule in tetrahedral field ($\tilde{K}/B = 1.33$ $B/\tilde{B} = 1.84$) is found more freer than in octahedral symmetry ($\tilde{K}/B = 20$ $B/\tilde{B} = 2.5$).

Another important result achieved is that only two levels with low energy ($A_1 + T_2$) are obtained in contrast to the three levels ($A_{1g} + T_{1u} + T_{2g}$) for octahedral symmetry. This enables us to obtain a decrease in the occumpation of energy levels at lower temperatures and consequently a heat capacity peak comparable to experimental values in the low temperature region ($T < 1K$) is achieved. But in the case of the three level system of octahedral symmetry field, it predicts a rather high heat capacity anomalies quite different from experimental values.

So our proposition, the reduction of the symmetry of the local crystal field in which the diatomic molecule rotates to a tetrahedral one, is a good alternative for modifying DMM model. But for quantitative description of experimental results, it is quite necessary to study the effects of interaction between the rotation of the molecule and the relaxations of the surrounding host atoms.

[22] Bagatski, M.I. et al, Sov. J. Low Temp. Phys., V.13, p.242 (1987)

[23] McWeeny, R., "Symmetry", Pergamon Press, Oxford (1963)

[24] Ballhausen, C.J., "Introduction to Ligand Field Theory", McGraw Hill, Inc., New York (1962)

[25] Cundy, H.M., Proc. Roy. Soc. A, V.164, p.420 (1938)

[26] Murmotsev, P.I. et al, Physico Technical Institute of Low Temperature, Acadamy of Sciences of Ukraine, Kharkov, (1991)